Cell Reports

Article

# Bacterial genotoxins induce T cell senescence

## Graphical abstract

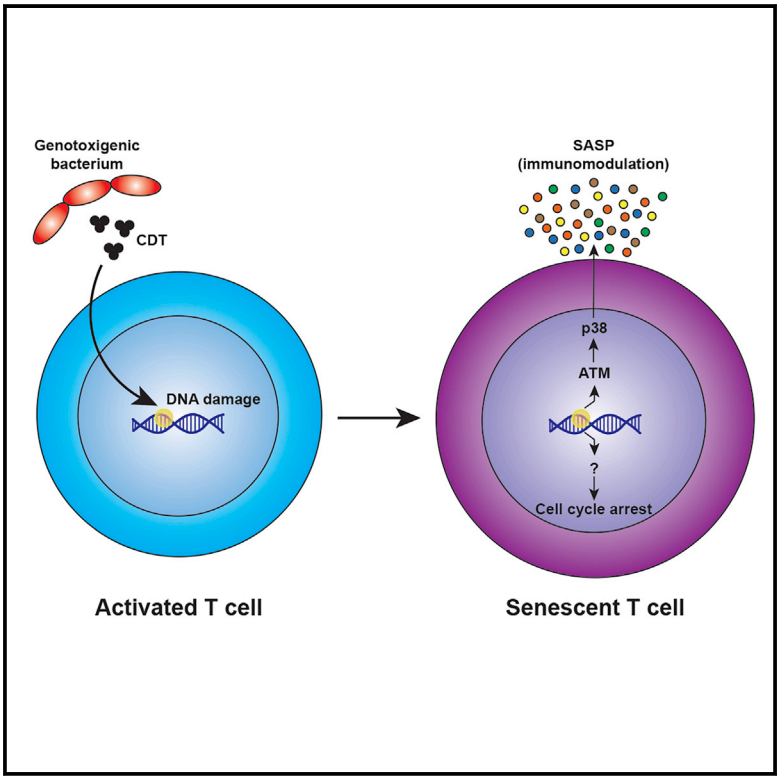


## Authors

Sarah L. Mathiasen, Laura Gall-Mas, Ioannis S. Pateras, ..., Teresa Frisan, Niels Ødum, Thorbjørn Krejsgaard

## Correspondence

thorkr@sund.ku.dk

## In brief

Mathiasen et al. show that the bacterial genotoxin CDT induces senescence and a senescence-associated secretory phenotype (SASP) in T cells. The SASP is orchestrated by the ATM-p38 axis, whereas the induction of senescence is ATM independent. Together, the findings uncover a putative link between genotoxigenic bacteria, T cell senescence, and immunomodulation.

## Highlights

- The bacterial genotoxin CDT induces senescence and a SASP in activated CD4 T cells
- ATM plays a key role in orchestrating the SASP but not in the induction of senescence
- ATM orchestrates the SASP via downstream activation of the p38 MAPK
- Infection with genotoxigenic bacteria increases the proportion of GL13$^{+}$ T cells *in vivo*

Mathiasen et al., 2021, Cell Reports *35*, 109220
June 8, 2021 
https://doi.org/10.1016/j.celrep.2021.109220

CellPress

Cell Reports

CellPress
OPEN ACCESS

Article

# Bacterial genotoxins induce T cell senescence

Sarah L. Mathiasen,[1,10] Laura Gall-Mas,[1,10] Ioannis S. Pateras,[2,10] Sofia D.P. Theodorou,[2] Martin R.J. Namini,[1] Morten B. Hansen,[3] Océane C.B. Martin,[4] Chella Krishna Vadivel,[1] Konstantinos Ntostoglou,[2] Deborah Butter,[4] Michael Givskov,[5] Carsten Geisler,[1] Arne N. Akbar,[6] Vassilis G. Gorgoulis,[2,7,8] Teresa Frisan,[4,9] Niels Ødum,[1] and Thorbjørn Krejsgaard[1,11,*]

[1]LEO Foundation Skin Immunology Research Center, Department of Immunology and Microbiology, University of Copenhagen, 2200 Copenhagen, Denmark
[2]Molecular Carcinogenesis Group, Department of Histology and Embryology, School of Medicine, National Kapodistrian University of Athens, 11527 Athens, Greece
[3]Department of Clinical Immunology, Rigshospitalet, Copenhagen University Hospital, 2100 Copenhagen, Denmark
[4]Department of Cell and Molecular Biology, Karolinska Institutet, 17177 Stockholm, Sweden
[5]Costerton Biofilm Center, Department of Immunology and Microbiology, University of Copenhagen, 2200 Copenhagen, Denmark
[6]Division of Medicine, University College London, London WC1E 6JF, UK
[7]Biomedical Research Foundation of the Academy of Athens, 11527 Athens, Greece
[8]Faculty Institute for Cancer Sciences, Manchester Academic Health Sciences Centre, University of Manchester, Manchester M13 9PL, UK
[9]Department of Molecular Biology and Umeå Center for Microbial Research (UCMR), Umeå University, 90187 Umeå, Sweden
[10]These authors contributed equally
[11]Lead contact
*Correspondence: thorkr@sund.ku.dk
https://doi.org/10.1016/j.celrep.2021.109220

## SUMMARY

Several types of pathogenic bacteria produce genotoxins that induce DNA damage in host cells. Accumulating evidence suggests that a central function of these genotoxins is to dysregulate the host's immune response, but the underlying mechanisms remain unclear. To address this issue, we investigated the effects of the most widely expressed bacterial genotoxin, the cytolethal distending toxin (CDT), on T cells—the key mediators of adaptive immunity. We show that CDT induces premature senescence in activated CD4 T cells *in vitro* and provide evidence suggesting that infection with genotoxin-producing bacteria promotes T cell senescence *in vivo*. Moreover, we demonstrate that genotoxin-induced senescent CD4 T cells assume a senescence-associated secretory phenotype (SASP) which, at least partly, is orchestrated by the ATM-p38 signaling axis. These findings provide insight into the immunomodulatory properties of bacterial genotoxins and uncover a putative link between bacterial infections and T cell senescence.

## INTRODUCTION

As part of their multifaceted infection program, many pathogenic bacteria express factors that directly or indirectly induce DNA damage in host cells (Chumduri et al., 2016; Gagnaire et al., 2017). Despite mounting evidence demonstrating that there exists an intrinsic cross-talk between the signaling pathways of the DNA-damage response (DDR) and the immune response, the effects of bacterial-induced DNA damage on host immunity are not well understood (Pateras et al., 2015).

One of the central ways bacteria can induce DNA damage in host cells is via the expression of genotoxins (Chumduri et al., 2016). The most widely expressed bacterial genotoxin is the cytolethal distending toxin (CDT), which is produced by a range of pathogenic Gram-negative bacterial species including *Campylobacter jejuni*, *Helicobacter hepaticus*, *Aggregatibacter actinomycetemcomitans*, *Shigella dysenteriae*, *Escherichia coli*, and *Haemophilus ducreyi*. The holotoxin is an exotoxin composed of three subunits: CdtA, CdtB, and CdtC. CdtB is the catalytically active subunit, which induces DNA damage, whereas CdtA and CdtC mediate the binding of the holotoxin to target cells. Once the holotoxin binds, CdtB and CdtC are endocytosed and retrogradely transported through the Golgi apparatus and endoplasmic reticulum. From there, CdtB is finally delivered to the nucleus where it induces DNA breaks. Besides CDT, the typhoid toxin (TT) produced by *Salmonella enterica* serovar Typhi also contains a catalytic CdtB subunit and functions as a protein genotoxin that damages DNA in host cells. The selective expression of CdtB by diverse pathogenic bacteria, together with the high conservation of key residues in the catalytic domain, strongly indicates that the enzymatic activity promotes bacterial virulence (Lara-Tejero and Galán, 2000; Nesić et al., 2004; Guerra et al., 2011a; Jinadasa et al., 2011; DiRienzo, 2014; Taieb et al., 2016; Scuron et al., 2016; Faïs et al., 2016). Accordingly, CDT has been shown to promote bacterial colonization, invasiveness, and persistent infection *in vivo* (Ge et al., 2008; McAuley et al., 2007). These findings raise the intriguing question: how can bacteria benefit from tampering with the genome in host cells?

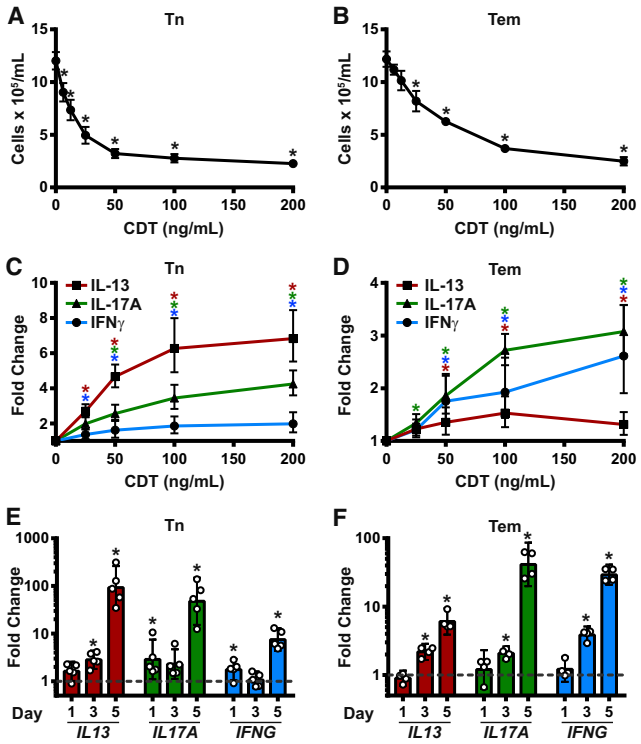


**Figure 1. CDT increases the secretion of signature effector cytokines from activated CD4 T cells**

(A–D) Tn and Tem cells were cultured with αCD3/CD28 beads and different concentrations of CDT. After 5 days, the numbers of live cells were counted and the concentrations of IL-13, IL-17, and IFNγ measured in the cell culture supernatants by ELISA. *Denotes a significant difference ($p < 0.05$) relative to cells cultured without CDT using a 1-way ANOVA with Dunnett's multiple comparisons test.

(A and B) Mean concentration of live cells ± SEM (n = 5).

(C and D) Fold change in the concentrations of IL-13, IL-17, and IFNγ relative to cells cultured without CDT. Shown is the geometric mean and 95% confidence interval (CI) (n = 6).

(E and F) Tn and Tem cells were cultured with αCD3/CD28 beads ± 200 ng/mL CDT for 1, 3, and 5 days before the relative levels of *IL13*, *IL17A*, *IFNG*, and *GAPDH* mRNA were determined by qPCR. The levels of *IL13*, *IL17A*, and *IFNG* mRNA were normalized to that of the reference gene *GAPDH* and depicted as the fold change in cells cultured with CDT relative to cells cultured without the toxin at the same time point. Circles depict the fold change in cytokine expression in cells from individual donors, bars represent the geometric mean, and error bars the 95% CI (n = 4–5). *Denotes a significant difference ($p < 0.05$) using a 2-way ANOVA with Sidak's multiple comparisons test.

See also Figure S1.

Providing a possible answer to this question, accumulating data suggest that bacteria can utilize targeted DNA damage as a strategy to subvert host immunity (Chumduri et al., 2016). Accordingly, CDT has been shown to target immune cells *in vitro* and promote inflammation *in vivo* (Faïs et al., 2016; Ge et al., 2008; Fox et al., 2004; Wising et al., 2005b; Shen et al., 2009; Scuron et al., 2016), whereas a functional TT has been shown to suppress intestinal inflammation and favor persistent infection (Del Bel Belluz et al., 2016). CDT-induced inflammation is suspected of contributing to various human pathologies including cancer, but the mechanisms underlying the immunomodulatory effects of bacterial genotoxins toxins are incompletely characterized (Guerra et al., 2011a; Scuron et al., 2016; Faïs et al., 2016; Ge et al., 2008; Shen et al., 2009; Martin and Frisan, 2020).

T cells exhibit particular high sensitivity to CDT intoxication when compared to other cell types, implying that a central function of the genotoxin is to target the adaptive immune response (Shenker et al., 1999; Wising et al., 2005a; Dixon et al., 2015; Scuron et al., 2016). Numerous studies have shown that CDT triggers a brief arrest in the G2 phase of the cell cycle rapidly followed by apoptotic cell death in malignant T cell lines (typically within 24 h) (Ohara et al., 2004, 2008; Wising et al., 2005a; Shenker et al., 2006; Chen et al., 2017). Apoptosis is classically considered an immunological silent form of cell death (Jorgensen et al., 2017), suggesting that CDT-mediated genotoxicity quickly eliminates T cells and, in apparent contrast to the proinflammatory properties of the toxin, suppresses T cell-mediated inflammation. Data from early studies, however, indicate that the toxin do not induce a rapid apoptotic response in activated primary T cells but rather cell-cycle arrest (Shenker et al., 1999, 2000). CDT was reported to induce apoptosis in a proportion of mitogen-stimulated human peripheral blood mononuclear cells (PBMCs) after prolonged exposure, but even after 3 days of culture, the large majority of intoxicated PBMCs stimulated with anti-CD3 and anti-CD28 antibodies did not exhibit DNA fragmentation (Shenker et al., 2001; Ohara et al., 2004). Therefore, we set out to shed light on the long-term effects of the genotoxin on the inflammatory response and fate of primary T cells.

## RESULTS

### CDT increases the secretion of signature effector cytokines from activated CD4 T cells

Initially, we aimed to clarify if activated primary T cells could survive prolonged exposure to CDT and address how intoxication influenced their inflammatory response. To this end, naive (Tn) and effector memory (Tem) CD4 T cells were isolated from the blood of healthy donors and cultured with activating anti-CD3/CD28 (αCD3/CD28) beads and different concentrations of CDT. Both Tn and Tem cells were studied to examine how the genotoxin influences the activation and differentiation of naive T cells as well as the activation and inflammatory response of activated memory T cells. After 5 days, the numbers of live cells were determined alongside with the supernatant concentrations of the three signature T helper (Th) cell effector cytokines interferon (IFN)γ (Th1), interleukin (IL)-13 (Th2), and IL-17 (Th17). CDT intoxication led to a dose-dependent decrease in the numbers of Tn and Tem cells, indicating that the toxin inhibited their proliferation and/or induced cell death (Figures 1A and 1B). However, even at high concentrations of the toxin, a considerable population of viable Tn and Tem cells was still present after 5 days of CDT exposure (Figures 1A and 1B). Despite the significant decrease in cell numbers, CDT strikingly induced a dose-dependent increase in the concentrations of IL-13, IL-17, and IFNγ in the cell culture supernatants (Figures 1C and 1D). This was not merely due to unspecific release of cytokines from ruptured apoptotic bodies or necrotic cells because the genotoxin also induced a vigorous upregulation of all three effector

cytokines at the mRNA level (Figures 1E and 1F). The increase in effector cytokine expression predominantly occurred after 3 days of intoxication, highlighting that it primarily was a delayed rather than an immediate effect (Figures 1E and 1F). As seen in Figures 1C–1F, CDT caused the greatest increase in the expression of IL-13 and IL-17A in activated Tn cells, whereas it preferentially increased the expression of IFNγ and IL-17A in activated Tem cells. However, the finding that CDT increased the expression of all three signature effector cytokines in both activated Tn and Tem cells indicated a general proinflammatory effect of the genotoxin on CD4 T cells. In contrast, a mutated form of CDT, devoid of DNase activity, did not affect the expression of the three effector cytokines from activated Tem cells, demonstrating that the proinflammatory effect is associated with the catalytic activity of the toxin (Figure S1). Moreover, CDT did not elicit secretion of the three effector cytokines from non-activated Tem cells, suggesting that the toxin selectively enhances the inflammatory response in activated CD4 T cells (Figure S1).

## CDT induces DNA damage, DDR activation, and irreversible cell-cycle arrest in activated CD4 T cells

CDT has been shown to trigger rapid apoptotic death in various malignant T cell lines (Shenker et al., 2006; Wising et al., 2005a; Ohara et al., 2004, 2008; Chen et al., 2017). Apoptosis is usually an immunological silent form of cell death not associated with increased expression of inflammatory factors (Jorgensen et al., 2017). Yet, we observed viable cells and highly increased expression of effector cytokines after 3–5 days of CDT intoxication, indicating that the toxin triggered a different cellular response in primary CD4 T cells from healthy donors. The cell line that has been most frequently used in studies investigating the effects of CDT on T cells is the Jurkat T cell line, an immortalized human leukemic cell line. In agreement with these studies (Wising et al., 2005a; Ohara et al., 2004; Shenker et al., 2006; Chen et al., 2017), we found that CDT caused extensive cell death in Jurkat T cells after 24 h of exposure, and after 48 h, virtually all cells were dead (Figure S2A). Conversely, CDT did not induce cell death in activated Tn cells within this time frame, underscoring that primary T cells respond differently to CDT-intoxication than Jurkat T cells (Figure S2B).

To shed light on the mechanisms underlying the proinflammatory effect of CDT on activated CD4 T cells, we characterized the cellular response of Tn and Tem cells to CDT intoxication in more detail. We first examined the phosphorylation status of ataxia-telangiectasia mutated (ATM) at serine 1981 and histone H2AX at serine 139 (also known as γH2AX); two prototypic biomarkers reflecting double-strand break (DSB) formation and DDR-activation. As shown in Figures 2A and 2B, CDT induced increased levels of both phosphorylated ATM and γH2AX in activated Tn and Tem cells relative to activated control T cells cultured without toxin. CDT intoxication further induced expression of phosphorylated p53 (Ser15), altogether validating that the toxin generated DNA damage and triggered the DDR in activated Tn and Tem cells (Figures 2A and 2B). The *CDKN1A* gene, which encodes the cyclin-dependent kinase (CDK) inhibitor $p21^{CIP1/WAF1}$, is a direct downstream target of p53 transactivation. In agreement with the upregulation of p53, CDT intoxication increased the levels of *CDKN1A* mRNA in activated Tn and Tem cells resulting in intense nuclear expression of $p21^{CIP1/WAF1}$ (Figures 2C, 2D, 2G, 2H, S2C, and S2D). Although the expression of $p21^{CIP1/WAF1}$ increased between 3 and 5 days of culture with CDT, the expression of p53 strongly decreased, suggesting that other factors played a central role in driving the expression of $p21^{CIP1/WAF1}$ in the later phases of intoxication (Figures 2A, 2B, 2G, and 2H). At 5 days post-intoxication, $p21^{CIP1/WAF1}$ induction was associated with enhanced expression of the CDK inhibitor $p16^{INK4a}$ in both Tn and Tem cells (Figures 2E–2H). Analyses of different toxin concentrations and time points demonstrated that CDT potently induced increased expression of $p21^{CIP1/WAF1}$, γH2AX, and $p16^{INK4a}$ in a concentration- and time-dependent manner (Figures S2E and S2F). Increased levels of these proteins are frequently used as markers of cellular senescence that is a state characterized by irreversible cell-cycle arrest (Sharpless and Sherr, 2015). Accordingly, CDT significantly inhibited the expression of the proliferation marker *MKI67* in activated Tn and Tem cells when compared to control T cells cultured without toxin (Figures 2I and 2J). Analysis of the cell-cycle distribution demonstrated that CDT increased the proportion of cells in G2/M phase (4*n*) at day 3 post-intoxication. Five days post-intoxication, this was followed by acquisition of polyploidy (*8n*) in a minor population of cells and a rise in sub-G1 cells (<2*n*) indicating increased cell death (Figure 2K). A considerable fraction of intoxicated cells was, however, still present in G0/G1 phase (2*n*) of the cell cycle (Figure 2K). These data suggest that CDT intoxication induces a prolonged cell-cycle arrest in the G1 and G2/M phases of the cell cycle followed by late cell death in a substantial fraction of the intoxicated cells.

To directly track the number of cell divisions at the single-cell level, we stained Tn and Tem cells with CellTrace Violet and cultured them with or without αCD3/CD28 beads and CDT for 5 days before analyzing the dilution of the dye in viable cells by flow cytometry. As shown in Figures 2L and 2M, activated Tn and Tem cells cultured without toxin had generally undergone multiple cell divisions. In sharp contrast, viable activated Tn and Tem cells cultured with CDT had not undergone any cell divisions similarly to non-activated T cells (Figures 2L and 2M). Failure to undergo cell division was not due to inhibition of the αCD3/CD28-mediated activation per se, as reflected by the similar upregulation of the activation marker CD45RO in Tn cells, independently of CDT treatment (Figure 2L). Collectively, these results support that CDT intoxication arrests activated primary CD4 T cells in both the G1 and G2/M phases of the cell cycle. This cell-cycle arrest appeared irreversible because activated Tn cells that had been cultured with CDT for 3 days did not re-enter the cell cycle upon subsequent restimulation with αCD3/CD28 beads in fresh culture media without CDT (Figure 2N). Because irreversible cell-cycle arrest is a characteristic of cellular senescence (Sharpless and Sherr, 2015), these findings indicate that CDT induces a state of stress-induced premature senescence (SIPS) in activated CD4 T cells.

## CDT promotes phenotypic traits of senescence in activated CD4 T cells

To substantiate this conclusion, we examined if CDT promoted a senescent phenotype in activated Tn and Tem cells. A common morphological feature of senescent cells is that they exhibit

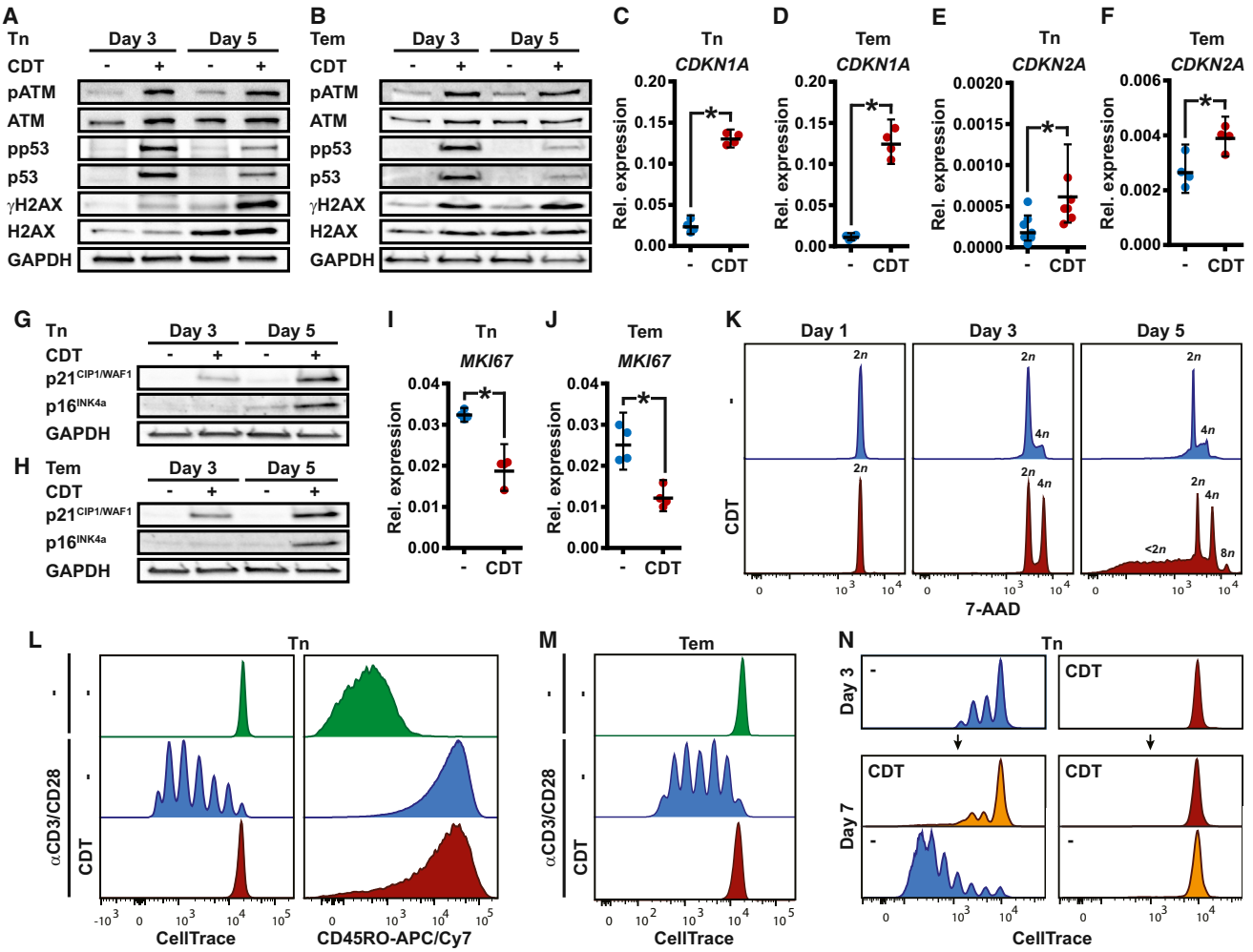


**Figure 2. CDT induces DNA damage, DDR activation, and irreversible cell-cycle arrest in activated CD4 T cells**

(A–J) Tn and Tem cells were cultured with αCD3/CD28 beads ± 200 ng/mL CDT.

(A and B) Western blots showing the protein levels of pATM (Ser1981), ATM, pp53 (Ser15), p53, γH2AX (Ser139), H2AX, and GAPDH (loading control) in Tn and Tem cells after 3 and 5 days of culture.

(C–F) qPCR analysis showing the expression of *CDKN1A* and *CDKN2A* mRNA relative to that of the reference gene *GAPDH* in Tn and Tem cells after 5 days of culture. Circles represent data points from individual donors, horizontal lines the geometric mean, and error bars the 95% CI (n = 4–6). *Denotes a significant difference ($p < 0.05$) using a paired t test.

(G and H) Western blots showing the protein levels of $p21^{CIP1/WAF1}$, $p16^{INK4a}$, and GAPDH in Tn and Tem cells after 3 and 5 days of culture. Each blot is representative of data from 3 donors.

(I and J) qPCR analysis showing the expression of *MKI67* mRNA relative to that of the reference gene *GAPDH* in Tn and Tem cells after 5 days of culture. Circles represent data points from individual donors, horizontal lines the geometric mean, and error bars the 95% CI (n = 4). *Denotes a significant difference ($p < 0.05$) using a paired t test.

(K) Tn cells were cultured with αCD3/CD28 beads ± 200 ng/mL CDT for 1, 3, and 5 days. The cells were subsequently permeabilized, stained with the DNA binding dye 7-AAD and the cellular DNA content analyzed by flow cytometry to examine the cell cycle distribution. The data are representative of 3 donors.

(L and M) Tn and Tem cells were stained with CellTrace Violet and cultured ± αCD3/CD28 beads and 200 ng/mL CDT for 5 days. The cellular dilution of CellTrace Violet was subsequently analyzed by flow cytometry to track the number of cell divisions. Tn cells were in addition stained with an antibody against CD45RO prior to flow cytometric analysis to examine their activation state. The histogram plots are each representative of 3 donors.

(N) Tn cells were stained with CellTrace Violet and cultured with αCD3/CD28 beads ± 200 ng/mL CDT for 3 days. Then, the cells were washed extensively and cultured without αCD3/CD28 beads and CDT for 1 day. The cells were finally restimulated with αCD3/CD28 beads and cultured in combinations ± 200 ng/mL CDT for 3 days further. The flow cytometric histogram plots are representative of 3 donors and display the dilution of CellTrace Violet in viable cells at day 3 and 7. (K–N) Histograms show the fluorescent intensity on the x axis and the number of events normalized to mode on the y axis.

See also Figure S2.

increased cell size (Sharpless and Sherr, 2015). Accordingly, a proportion of activated Tn and Tem cells displayed considerably increased cell size after 5 days of culture with CDT when compared to activated Tn and Tem cells cultured without toxin (Figures 3A, S3A, and S3B). Conforming to the phenotype of senescent CD4 T cells, intoxicated Tn and Tem cells further expressed decreased levels of the co-stimulatory molecule CD27 and elevated levels of the cell surface receptor CD45RA relative to activated control T cells (Figures 3B–3E and S3B–S3E) (Xu and Larbi, 2017). Moreover, CDT intoxication increased the mRNA levels of granzyme B (*GZMB*) and perforin-1 (*PRF1*), which are upregulated in senescent CD4 T cells (Figures 3F and 3G) and decreased the mRNA levels of lamin B1 (*LMNB1*) and aurora kinase B (*AURKB*), which are downregulated in cells undergoing senescence (Figures S3F and S3G) (Akbar et al., 2016; Kuwahara et al., 2014; Covre et al., 2019; Freund et al., 2012; Kim et al., 2011). Finally, we cultured activated Tn cells in absence or presence of CDT for 5 days and stained them with the compound GL13 (also termed SenTraGor), which detects lipofuscin with high sensitivity and specificity (Evangelou et al., 2017). Lipofuscin is a non-degradable aggregate of oxidized proteins, lipids, and metals that accumulates in the cytoplasm of senescent cells and, thus, provides a robust biomarker for cellular senescence (Georgakopoulou et al., 2013). As shown in Figures 3H and 3I, CDT induced a strong increase in the percentage of GL13-positive cells relative to activated Tn cells cultured without toxin, altogether supporting that CDT induces SIPS in activated CD4 T cells.

An important feature distinguishing senescent cells from non-senescent cell-cycle-arrested cells is that they typically acquire a senescence-associated secretory phenotype (SASP)—a phenomenon characterized by highly increased expression of a wide array of secreted proteins including inflammatory mediators (Coppé et al., 2008; van Deursen, 2014). Therefore, we investigated if the CDT-mediated increase in signature effector cytokine secretion from activated Tn and Tem cells (Figures 1C–1F) reflected acquisition of a SASP. We focused on the expression of cytokines and chemokines as they are among the most highly conserved SASP components across cell types and senescence-inducing stimuli (van Deursen, 2014). As seen in Figures 3J and 3K, activated Tn and Tem cells cultured with CDT for 5 days expressed highly increased mRNA levels of a broad range of cytokines and chemokines relative to activated control cells cultured without toxin. Of the 25 examined cytokines and chemokines, 21 were upregulated in intoxicated Tn cells and 23 were upregulated in intoxicated Tem cells, demonstrating that CDT induces a SASP in activated CD4 T cells (Figures 3J and 3K). The main differences in the SASP profile between intoxicated Tn and Tem cells were that CDT induced significantly increased expression of *IL7* mRNA in Tn cells but not in Tem cells, whereas the toxin induced significantly increased expression of *TNFA*, *IL15*, and *IL32* mRNA in Tem cells but not in Tn cells (Figures 3J and 3K). In line with our prior findings, CDT further tended to induce a greater increase in the mRNA expression of the Th1 cytokine IFNγ in Tem cells than in Tn cells, whereas the increases in the mRNA levels of the Th2 cytokines IL-4, IL-5, and IL-13 tended to be greater in Tn cells than in Tem cells (Figures 3J and 3K). In both intoxicated Tn and Tem cells, three of the genes that were most abundantly upregulated at the mRNA level were *IL9*, *CCL1*, and *IL17* (Figures 3J and 3K). Supporting that the observed mRNA changes were translated to the protein level, the concentrations of IL-9, CCL1, and IL-17 were also strongly increased in supernatants from activated Tn and Tem cells exposed to CDT when compared to supernatants from activated control T cells (Figures 1C, 1D, and 3L–3O).

## The ATM-p38 axis plays a central role in orchestrating the CDT-induced SASP in activated CD4 T cells

Whereas the mechanisms driving the SASP have been a matter of intense investigation in non-immune cells (Tchkonia et al., 2013), little is known about these mechanisms in senescent T cells and whether they are equivalent to those identified in fibroblasts and epithelial cells. Consequently, we next sought to shed light on the signaling pathways that drives the genotoxin-induced SASP in primary T cells.

ATM is at the core of the DDR machinery and has been shown to play an important role in orchestrating the SASP in fibroblasts (Rodier et al., 2009; Kang et al., 2015; Zhang et al., 2018). Therefore, we initially assessed if the SASP was dependent on the activation of ATM in genotoxin-intoxicated T cells. H2AX is a direct target of ATM in response to DSBs, and accordingly, the selective ATM inhibitor, KU-60019, reduced the CDT-induced elevation of γH2AX in activated Tn cells (Figure 4A). In parallel, the inhibitor almost completely abrogated the CDT-induced secretion of CCL1, IL-9, and IL-17 with no or little influence on the secretion of these factors from activated control Tn cells (Figure 4B). Interestingly, the inhibitor did not have a significant effect on the numbers of live cells (Figures 4C and S4A) or the percentages of GL13- and $p16^{INK4a}$-positive cells upon CDT exposure (Figures S4B–S4D). Collectively, these findings suggest that ATM plays a central role in orchestrating the SASP in CDT-intoxicated T cells but not in the induction of senescence per se.

CDT has been shown to induce phosphorylation of the mitogen-activated protein kinase (MAPK) p38 in epithelial cells, and a recent study suggested that p38 governs the SASP in senescent CD8 T cells (Callender et al., 2018; Guerra et al., 2008). Accordingly, we next examined if p38 was active and promoted the SASP in intoxicated CD4 T cells. As shown in Figure 4D, CDT increased the phosphorylation of p38 in activated Tn cells after 48 and 72 h of culture, indicating that the toxin triggered a delayed increase in the activity of p38 that preceded the SASP. Phosphorylated p38 accumulated in the nucleus of intoxicated cells, implying that the protein may modulate the activity of nuclear factors in response to CDT intoxication (Figures 4E and S4E). Importantly, inhibition of ATM blocked the CDT-induced phosphorylation of p38 (Figure 4F), providing evidence that the delayed activation of p38 is ATM-dependent. To address if p38 promoted the SASP, activated Tn cells were cultured in absence or presence of CDT for 5 days with or without addition of the selective p38 inhibitor, SB203580, after 48 h of culture. As observed with the ATM inhibitor, SB203580 almost completely abolished the CDT-induced secretion of CCL1, IL-9, and IL-17 whereas it had no or minor effect on the secretion of these factors from activated control Tn cells (Figure 4G). Furthermore,

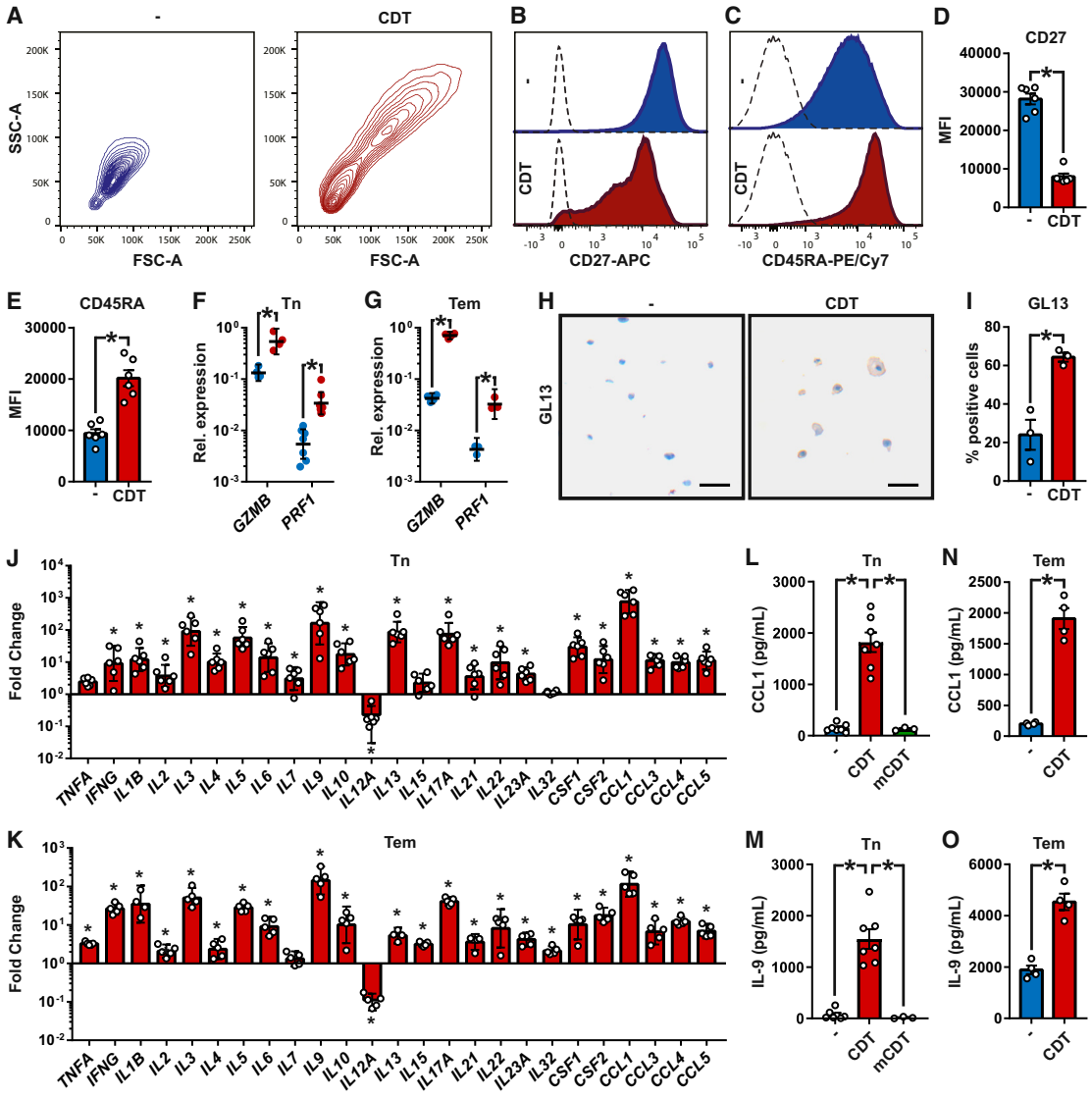


**Figure 3. CDT promotes phenotypic traits of senescence in activated CD4 T cells**

Tn and Tem cells were cultured for 5 days with αCD3/CD28 beads ± 200 ng/mL CDT or (L and M) 200 ng/mL mutated CDT (mCDT). Then, the cells were analyzed by (A–E) flow cytometry, (F, G, J, and K) qPCR or (H and I) immunocytochemistry, and (L–O) the cell culture supernatants by ELISA.

(A) Forward (FSC-A) and side-scatter (SSC-A) contour plots representative of data obtained using Tn cells from 6 donors.

(B and C) Representative histogram plots showing the relative expression of CD27 and CD45RA on Tn cells. Histograms show the fluorescent intensity on the x axis and the number of events normalized to mode on the y axis. Dotted lines represent unstained cells.

(D and E) Graphs summarizing the relative expression of CD27 and CD45RA on Tn cells from 6 donors. Circles depict the median fluorescent intensity (MFI) of cells from individual donors and bars the mean MFI ± SEM (n = 6).

(F and G) The expression of *GZMB* and *PRF1* mRNA relative to that of the reference gene *GAPDH* in activated Tn and Tem cells cultured without (blue circles) or with (red circles) CDT. Circles represent data points from individual donors, horizontal lines the geometric mean, and error bars the 95% CI (n = 4–6).

(H) Representative micrographs of Tn cells stained with GL13. Scale bar, 100 μm.

(I) Graph summarizing the percentages of GL13-positive Tn cells from 3 donors. Circles depict data points from individual donors and bars the mean ± SEM (n = 3).

(J and K) The mRNA levels of the indicated cytokines and chemokines were normalized to that of *GAPDH* and shown as fold change in cells cultured with CDT relative to cells cultured without CDT. Circles depict data points from individual donors, bars the geometric mean, and error bars the 95% CI (n = 4–6).

(L–O) The concentrations of CCL1 and IL-9 in cell culture supernatants from Tn and Tem cells. Circles depict data points from individual donors and bars the mean ± SEM (n = 4–7). *Denotes a significant difference ($p < 0.05$) using (D–G, I, and L–O) a paired t test or (J and K) a 2-way ANOVA with Sidak's multiple comparisons test.

See also Figure S3.

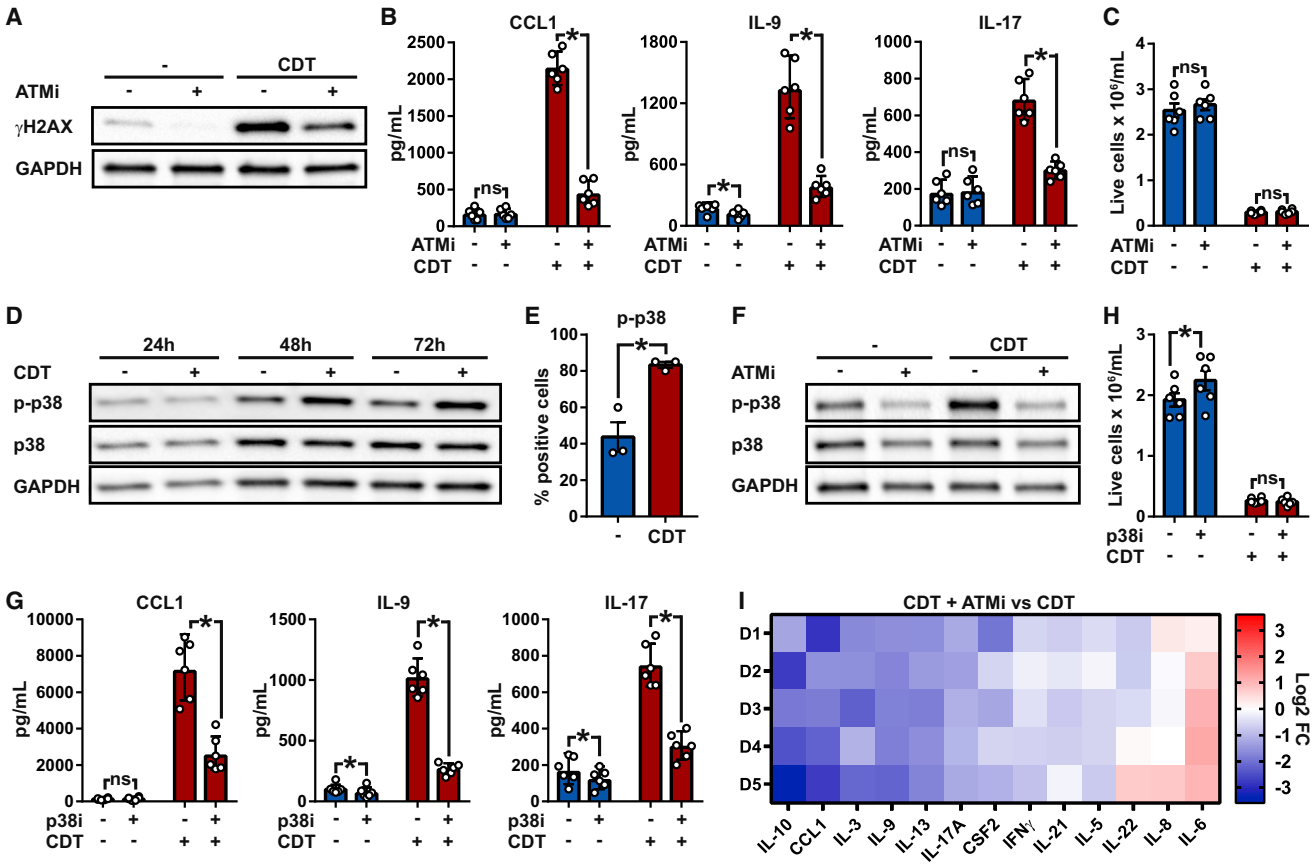


**Figure 4. The ATM-p38 axis plays a central role in orchestrating the CDT-induced SASP in activated CD4 T cells**

(A–C) Activated Tn cells were cultured with 3 μM ATM inhibitor (ATMi, KU-60019) or vehicle (–) for 5 days ± 200 ng/mL CDT.

(A) Western blot showing the levels of γH2AX and GAPDH (loading control). The blot is representative of 3 donors.

(B) The concentrations of CCL1, IL-9, and IL-17 in the cell culture supernatants (n = 6).

(C) Histogram showing the concentrations of live cells (n = 6).

(D) Western blot showing the levels of p38 phosphorylated on Thr180/Tyr182 (p-p38), total p38, and GAPDH in Tn cells cultured for 24, 48, and 72 h with αCD3/CD28 beads ± 200 ng/mL CDT. The blot is representative of 4 donors.

(E) Graph summarizing the percentages of Tn cells positive for nuclear p-p38 after 5 days of culture with αCD3/CD28 beads ± 200 ng/mL CDT (n = 3).

(F) Western blot showing the levels of p-p38, p38, and GAPDH in Tn cells cultured for 5 days with αCD3/CD28 beads ± 200 ng/mL CDT and 3 μM KU-60019 (ATMi). The blot is representative of 3 donors.

(G and H) Tn cells were cultured with αCD3/CD28 beads ± 200 ng/mL CDT. After 48 h of culture, 10 μM p38 inhibitor (p38i, SB203580) or vehicle (–) was added, and the cells were cultured 72 h more for a total of 5 days prior to analysis.

(G) The concentrations of CCL1, IL-9, and IL-17 in the cell culture supernatants (n = 6).

(H) Histogram showing the concentrations of live cells (n = 6).

(I) Tn cells from 5 donors (D1–D5) were cultured with αCD3/CD28 beads and 200 ng/mL CDT in presence of 3μM ATMi or vehicle for 5 days. Subsequently, the concentrations of the respective cytokines were determined in the cell culture supernatants by ELISA. The heatmap illustrates the log2 fold change (FC) in the concentration of the given cytokine in supernatants from cells cultured with CDT + ATMi relative to the concentration in supernatants from cells cultured with CDT + vehicle. (B, C, E, G, and H) Circles represent data points from individual donors and bars the mean ± SEM. *Denotes a significant difference ($p < 0.05$) and no significant (ns) difference ($p > 0.05$) using a paired t test.

See also Figure S4.

inhibition of p38 did not influence the CDT-mediated decrease in cell numbers (Figure 4H) and had little or no effect on the expression of examined senescence-associated markers (Figures S4F and S4G), supporting that p38 governs the SASP in T cells (Callender et al., 2018) but is dispensable for the capacity of CDT to trigger T cell senescence. Together, these data indicate that ATM, at least partially, orchestrates the SASP via activation of p38.

To gain a broader picture of the role of the ATM-p38 axis in regulating the SASP, we next selected a panel of the cytokines that were induced by CDT (Figures 3J and 3K) and analyzed their concentrations in supernatants from activated Tn cells cultured with CDT in presence of ATM inhibitor or vehicle. As seen in Figure 4I, blocking the activity of ATM strongly inhibited the secretion of the majority of the analyzed cytokines from CDT-intoxicated T cells. However, we did observe some donor-specific

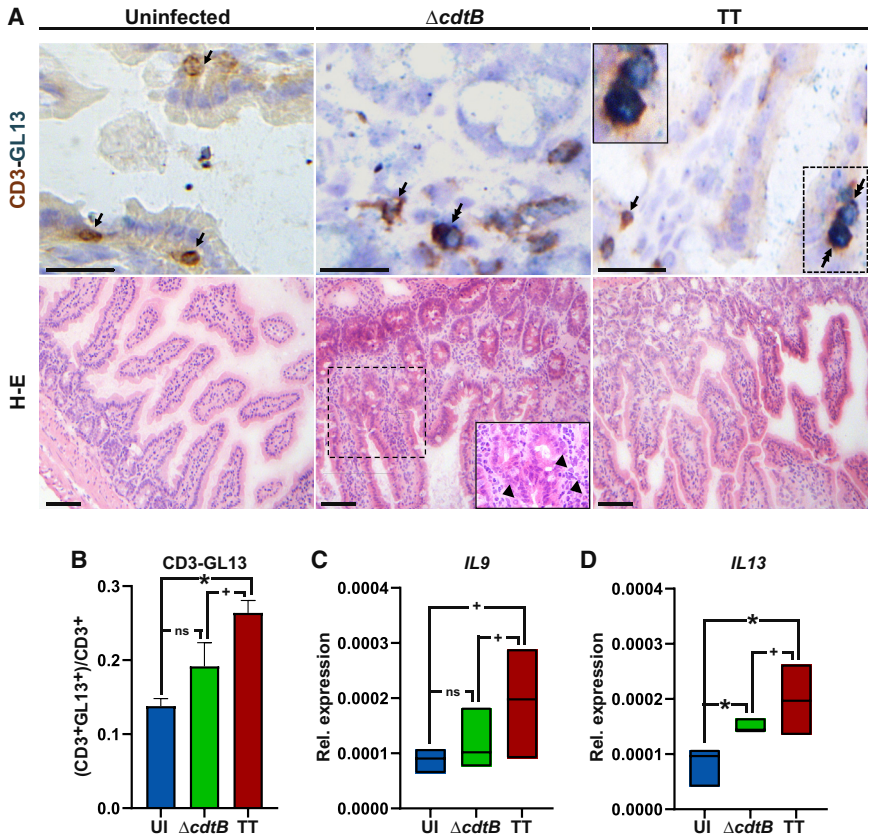


**Figure 5. Elevated proportion of senescent T lymphocytes in the small intestine of mice infected with *Salmonella* expressing a genotoxin**

(A) Upper panel shows representative micrographs from sequential CD3 (visualized with brown, single arrow) and GL13 (depicted with emerald) double immunostaining of intestinal tissue from uninfected mice or mice infected with MC1-Δ*cdtB* or MC1-TT. Double arrows demonstrate double-positive cells ($CD3^+GL13^+$). Scale bar, 50 μm. Inset in the TT micrograph zooms on double positive cells. The lower panel shows representative micrographs from H&E staining demonstrating increased severity of enteritis in the MC1-Δ*cdtB* cases. Scale bar, 100 μm. Inset in the Δ*cdtB* micrograph zooms on neutrophil infiltration indicated with arrowheads.

(B) Quantification of $(CD3^+GL13^+)/(CD3^+)$ ratios in uninfected (UI), Δ*cdtB*, and TT cases. Bars represent the mean + SEM (n = 3).

(C and D) Expression of *IL9* and *IL13* mRNA relative to that of the reference gene *Gapdh* in the small intestine of uninfected (UI) (n = 3), MC1-Δ*cdtB* (n = 5), and MC1-TT cases (n = 4). Horizontal lines depict the median and floating bars minimum and maximum.

(B–D) *$p < 0.05$, +$p < 0.15$, and ns, $p \geq 0.15$ using a Student's t test.

variation, and the ATM inhibitor also had no effect or even increased the secretion of a few cytokines. These findings corroborate that ATM plays a central role in orchestrating the genotoxin-induced SASP in T cells but concurrently indicate that other pathways contribute to the acquisition of a full-fledged SASP, and ATM may modulate the secretory profile by promoting or suppressing the expression of individual factors.

### Elevated proportion of senescent T lymphocytes in the small intestine of mice infected with *Salmonella* expressing a genotoxin

To validate the *in vitro* findings in an *in vivo* context, we utilized sv129 mice that were infected with the *Salmonella* Typhimurium strain MC1 harboring the TT genotoxin (MC1-TT) or an isogenic strain deficient of the genotoxin subunit CdtB (MC1-Δ*cdtB*). To examine the ability of the bacterial genotoxin to induce senescence in T cells, we performed a double sequential staining to visualize $CD3^+$ and $GL13^+$ cells on the same section in the small intestine of mice 10 days post infection. Tissues from mice infected with MC1-TT exhibited a significantly increased $(CD3^+GL13^+)/(CD3^+)$ ratio versus matched uninfected mice (Figures 5A and 5B). A small, albeit not statistically significant, increase was also observed in mice infected with the MC1-Δ*cdtB* strain when compared to uninfected mice (Figures 5A and 5B). The latter is consistent with the increased inflammatory response previously reported in these mice in comparison with the MC1-TT cases (Del Bel Belluz et al., 2016) and reproduced in this experimental set up (Figure 5A). Therefore, it is conceivable that the relative increase in T cells with a senescent phenotype is mediated by two different mechanisms: the bacterial genotoxin in the MC1-TT infected mice and inflammation-induced DDR in mice infected with the control strain (Aivaliotis et al., 2012). In line with the *in vitro* data demonstrating enhanced expression of IL-9 and IL-13 in T cells exposed to CDT, qPCR analysis revealed a tendency toward increased mRNA levels for *IL9* and *IL13* in mice infected with the genotoxigenic strain compared to the levels observed in mice infected with the MC1-Δ*cdtB S*. Typhimurium strain and uninfected mice (Figures 5C and 5D).

## DISCUSSION

Accumulating data suggest that bacteria can manipulate the immune response through the expression of factors that induce DNA damage in host cells (Chumduri et al., 2016; Gagnaire et al., 2017; Del Bel Belluz et al., 2016). Nevertheless, the effects of bacterial-induced DNA damage on primary immune cells remain poorly characterized. Here, we show that the bacterial genotoxin CDT induces SIPS and a SASP in activated primary CD4 T cells. Furthermore, we find an increased proportion of T cells with a senescent phenotype in the small intestine of mice infected with *S*. Typhimurium expressing TT when compared to control mice. Although bacterial genotoxins have been shown to trigger senescence in cells of epithelial and

mesenchymal origin (Blazkova et al., 2010; Kosar et al., 2011; Secher et al., 2013; Cougnoux et al., 2014), the present findings importantly contribute to the understanding of the immunomodulatory properties of bacterial genotoxins.

Previous studies have shown that CDT exposure triggers a brief G2 arrest rapidly followed by apoptotic cell death in various malignant T cell lines (Wising et al., 2005a; Ohara et al., 2004, 2008; Shenker et al., 2006; Chen et al., 2017). In the present work, we demonstrate that CDT induces prolonged cell-cycle arrest in activated primary CD4 T cells, which is accompanied by the acquisition of phenotypic characteristics of senescence. Because the cellular response to CDT intoxication is significantly influenced by the expression and functionality of factors involved in DNA damage and repair, cellular stress, proliferation, and survival, it seems very plausible that perturbations of such cellular pathways in malignant T cell lines may cause them to respond differently to the toxin than primary T cells from healthy donors (Fedor et al., 2013; Guerra et al., 2008; Shenker et al., 2001, 2006, 2007; Ohara et al., 2008; Bezine et al., 2016). In line with this conclusion, we found that CDT exposure induced extensive cell death in Jurkat T cells within 48 h of culture, whereas the toxin did not induce cell death in primary activated CD4 T cells within this time frame. Nevertheless, our findings do not exclude the possibility that some subtypes, or very high concentrations of CDT, can trigger rapid cell death in primary T cells without prior induction of SIPS.

Epithelial cells and fibroblasts characteristically enlarge in response to CDT intoxication but it had been reported not to be the case for T cells (Shenker et al., 1999, 2001). Yet, we observed an extensive increase in the size and granularity of a substantial proportion of activated CD4 T cells after 5 days of CDT intoxication. Prior studies notably investigated the size and granularity of activated T cells after 3 days of culture with CDT (Shenker et al., 1999, 2001). This could explain the apparent discordant results as we first observed increased cell size at later time points (i.e., simultaneous with the appearance of a senescent phenotype). Collectively, our results provide evidence showing that CDT induces increased cell size, prolonged cell-cycle arrest, and the expression of senescence-associated markers in primary T cells. Because these traits are also characteristic for intoxicated epithelial and mesenchymal cells, our findings highlight that a proportion of hematopoietic cells shows a similar cellular response to the toxin as cells of epithelial and mesenchymal origin—an issue that has been previously underrated (Gagnaire et al., 2017; Jinadasa et al., 2011; Grasso and Frisan, 2015; Taieb et al., 2016; Faïs et al., 2016; Gargi et al., 2012).

The proinflammatory properties of CDT are suspected of fueling various human pathologies (Guerra et al., 2011a; Faïs et al., 2016; Scuron et al., 2016; Ge et al., 2008; Fox et al., 2004; Wising et al., 2005b; Shen et al., 2009). Therefore, it is of particular interest to unravel the cellular mechanisms underlying the inflammatory effects of the toxin. Prior studies had reported that CDT triggers apoptotic cell death in T cells, indicating that the toxin would suppress T cell-mediated inflammation (Shenker et al., 2001, 2006; Wising et al., 2005a; Ohara et al., 2004, 2008; Chen et al., 2017). Interestingly, we found that CDT induces premature senescence and a SASP in activated primary T cells. Thus, even if the intoxicated cells should eventually succumb to the cytolethal actions of the toxin, these findings importantly suggest that the potent effects of CDT on T cells may contribute to the toxin's inflammatory properties *in vivo*. CDT did not induce expression of effector cytokines from resting T cells, indicating that the toxin exclusively elicits a SASP in activated T cells. It is an intriguing question if CDT-induced senescence and the accompanying SASP benefit the host or the bacteria. On one hand, the senescent state may facilitate or prolong the survival of activated T cells exposed to CDT, thereby allowing them to release a potent distress signal via the SASP that enhances the immune reaction against the intruding bacteria and promotes the clearance of damaged cells. On the other hand, CDT-producing bacteria could benefit from inducing increased inflammation in the face of an impaired adaptive immune response. Indeed, other bacterial toxins such as staphylococcal enterotoxins, which induce high secretion of inflammatory factors from T cells, while concurrently impairing their function, have been shown to enhance bacterial survival and persistent infection (Tuffs et al., 2018).

Whereas the SASP and its underlying mechanisms have been a subject of intense research in non-immune cells, it was first recently reported that human T cells with a senescent phenotype display a SASP (Callender et al., 2018; Covre et al., 2019; Tchkonia et al., 2013). The present work corroborates this finding by showing that genotoxin-induced senescence is associated with the development of a SASP in T cells. Directly connecting the CDT-triggered SASP with the DDR, inhibition of ATM impaired the toxin-induced secretion of the majority of the examined inflammatory factors. Previous studies have, accordingly, highlighted ATM as a pivotal player in orchestrating the molecular program driving the SASP in fibroblasts (Kang et al., 2015; Rodier et al., 2009; Zhang et al., 2018). In addition to its DNase activity, CDT has also been reported to harbor phosphatase activity (Dlakic, 2001; Shenker et al., 2007). Although the present results provide evidence that CDT-induced activation of the DDR plays a central role in orchestrating the SASP, they do not rule out that the induction of DNA damage and DDR activation could be triggered indirectly via the phosphatase activity of CDT and not directly via DNase-mediated genotoxicity. The fact that a catalytically inactive mutant of CDT did not induce expression of cytokines, however, confirmed that the SASP was triggered by the enzymatic activity of CdtB.

The MAPK p38 has been demonstrated to be a central driver of the SASP in fibroblasts, and p38 inhibition was recently shown to inhibit the SASP in CD8 T cells displaying a senescent phenotype (Freund et al., 2011; Callender et al., 2018). Accordingly, we observed that CDT intoxication led to a delayed increase in the phosphorylation and nuclear accumulation of p38 that preceded the SASP. As with inhibition of ATM activity, blockage of p38 activity abolished the CDT-induced secretion of CCL1, IL-9, and IL-17. Inhibition of ATM further prevented the delayed increase in p38 phosphorylation, suggesting that ATM at least partly orchestrates the CDT-induced SASP through activation of p38. In support of this conclusion, spontaneous activation of ATM has been shown to stimulate the activity of p38 in T cells with a senescent

phenotype, and a recent study reported that the ATM-TRAF6-TAK1 axis promotes the SASP via activation of p38 in human stromal cells exposed to genotoxic anti-cancer treatments (Zhang et al., 2018; Lanna et al., 2014).

In contrast to the SASP, our results suggest that CDT-induced T cell senescence is not dependent on activation of the ATM-p38 axis. Providing a putative explanation for this finding, CDT has not only been shown to activate ATM but also ATR in target cells (Fahrer et al., 2014). Because persistent activation of ATR is sufficient to induce cell-cycle arrest and cellular senescence, it is possible that ATR might play a central role in the induction of senescence in genotoxin-intoxicated T cells (Toledo et al., 2008). Indeed, Ibler et al. (2019) recently reported that TT induces a non-canonical DDR named RING in proliferating cells that drives cellular senescence and is characterized by accumulation of γH2AX at the nuclear periphery. This non-canonical DDR is caused by excessive DNA replication stress that exhausts the RPA pathway and is dependent on activation of ATR but not ATM (Ibler et al., 2019). We speculate that ATR may drive CDT-induced senescence in activated T cells via a similar mechanism.

The proportion of T cells with a senescent phenotype increases with age but varies among individuals (Akbar et al., 2016). In line with their impaired proliferative capacity and excessive production of inflammatory factors, senescent T cells have been proposed to play a role in pathologies arising from chronic inflammation and the declining immune function in elderly individuals (Callender et al., 2018; Macaulay et al., 2013; Chou and Effros, 2013; Yi et al., 2019). Latent viral infections are known to be associated with increased levels of T cells displaying a senescent phenotype. It is believed that reactivations of latent viral infections drive the accumulation of senescent T cells by recurrently triggering the proliferation of specific long-lived memory T cells leading to telomere erosion and, consequently, replicative senescence (Akbar and Henson, 2011). Yet, a substantial proportion of T cells displaying a senescent phenotype do not exhibit short telomeres, indicating the existence of telomere-independent triggers inducing premature T cell senescence (Akbar et al., 2016; Di Mitri et al., 2011). Beside viral infection, T cells with a senescent phenotype accumulate during cutaneous infection with the protozoan parasite *Leishmania braziliensis* (Covre et al., 2019), and the presents findings suggest a link between genotoxigenic bacteria and T cell senescence. Because genotoxin-induced senescent T cells may eventually die from the cytotoxic effects of the toxin or be targeted for immune-mediated destruction, further studies are needed to resolve if bacterial genotoxins can give rise to long-lived senescent T cells *in vivo*.

The significant increase of the $(CD3^+GL13^+)/(CD3^+)$ ratio in mice infected with the MC1-TT strain compared to uninfected mice supports that bacterial genotoxins have the capacity to induce T cell senescence *in vivo*. It has previously been shown that TT suppresses the inflammatory response in the small intestine of mice infected with *S*. Typhimurium (Del Bel Belluz et al., 2016). Accordingly, the small non-significant increase in the proportion of $CD3^+GL13^+$ cells detected in the intestine of mice infected with the MC1-Δ*cdtB* strain relative to uninfected mice may be due to the severity of inflammation and consequent oxidative stress-induced senescence (Gorgoulis et al., 2019). Whereas TT suppresses the inflammatory response in the small intestine in mice infected with *S*. Typhimurium, it enhances the inflammatory response in the liver (Del Bel Belluz et al., 2016). Based on our *in vitro* studies, this could partly be explained by the dual capacity of CdtB to promote inflammation by inducing a SASP and inhibit inflammation by inducing cell-cycle arrest and cell death in CD4 T cells. Additionally, CDT may induce a different SASP profile in different cell types, highlighting that the net effect of bacterial genotoxins on inflammation is highly complex and influenced by several factors *in vivo*.

In conclusion, we provide evidence linking bacterial genotoxins to the induction of senescence and a SASP in T cells. We further show that the ATM-p38 axis plays a central role in orchestrating the genotoxin-induced SASP, altogether shedding light on the immunomodulatory properties of bacterial genotoxins as well as the molecular pathways governing the SASP in T cells.

## STAR★METHODS

Detailed methods are provided in the online version of this paper and include the following:

- KEY RESOURCES TABLE
- RESOURCE AVAILABILITY
  - Lead contact
  - Materials availability
  - Data and code availability
- EXPERIMENTAL MODEL AND SUBJECT DETAILS
  - Mice
  - Primary human CD4 T cells
  - Jurkat T cell line
- METHOD DETAILS
  - Recombinant CDT and mCDT
  - Cell counting
  - Enzyme-Linked Immunosorbent Assay
  - QPCR analysis
  - Western blotting
  - Flow cytometry
  - Immunocytochemistry and immunohistochemistry
- QUANTIFICATION AND STATISTICAL ANALYSIS

## SUPPLEMENTAL INFORMATION

Supplemental information can be found online at https://doi.org/10.1016/j.celrep.2021.109220.

## ACKNOWLEDGMENTS

We would like to thank Eleni Paparouna for the technical support in the *in situ* assays. This work was supported by a Postdoctoral grant and a Sapera Aude Talent grant from the Independent Research Fund Denmark (DFF-4092-00122 to T.K.); the Danish Cancer Society (R56-A2924-12-S2 to T.K. and R221-A13193 to L.G.-M.); the Lundbeck Foundation (2015-486 to M.G.); the Swedish Cancer Society (CAN 2017/315 to T.F.); the Swedish Research Council (2018-02521 to T.F.); the Kempestiftelserna (JCK-1826 to T.F.); the Cancer Research Foundation in Northern Sweden (AMP 17-884 to T.F.); Umeå University (to T.F.); the Novo Nordisk Research Foundation (NNF14OC0012345 to N.Ø.); and the LEO Foundation. The funders had no role in study design, data collection and analysis, the decision to publish, or preparation of the manuscript.

## AUTHOR CONTRIBUTIONS

Conceptualization, I.S.P., T.F., and T.K.; methodology and expertise, I.S.P., M.B.H., M.G., C.G., A.N.A., V.G.G., T.F., N.Ø., and T.K.; investigation, S.L.M., L.G.-M., I.S.P., S.D.P.T., M.R.J.N., O.C.B.M., C.K.V., K.N., D.B., and T.K.; resources, M.B.H., M.G., V.G.G., T.F., and N.Ø.; writing – original draft, T.K.; writing – review & editing, S.L.M., L.G.-M., I.S.P., S.D.P.T., M.R.J.N., M.B.H., O.C.B.M., C.K.V., K.N., D.B., M.G., C.G., A.N.A., V.G.G., T.F., and N.Ø.; visualization, I.S.P., S.D.P.T., T.F., and T.K.; supervision, I.S.P., T.F., and T.K.; funding acquisition, T.F., N.Ø., and T.K. All authors approved the manuscript.

## DECLARATION OF INTERESTS

The authors declare no competing interests.

Received: August 8, 2019
Revised: February 16, 2021
Accepted: May 14, 2021
Published: June 8, 2021

## REFERENCES

Aivaliotis, I.L., Pateras, I.S., Papaioannou, M., Glytsou, C., Kontzoglou, K., Johnson, E.O., and Zoumpourlis, V. (2012). How do cytokines trigger genomic instability? J. Biomed. Biotechnol. *2012*, 536761.

Akbar, A.N., and Henson, S.M. (2011). Are senescence and exhaustion intertwined or unrelated processes that compromise immunity? Nat. Rev. Immunol. *11*, 289–295.

Akbar, A.N., Henson, S.M., and Lanna, A. (2016). Senescence of T Lymphocytes: Implications for Enhancing Human Immunity. Trends Immunol. *37*, 866–876.

Bezine, E., Malaisé, Y., Loeuillet, A., Chevalier, M., Boutet-Robinet, E., Salles, B., Mirey, G., and Vignard, J. (2016). Cell resistance to the Cytolethal Distending Toxin involves an association of DNA repair mechanisms. Sci. Rep. *6*, 36022.

Blazkova, H., Krejcikova, K., Moudry, P., Frisan, T., Hodny, Z., and Bartek, J. (2010). Bacterial intoxication evokes cellular senescence with persistent DNA damage and cytokine signalling. J. Cell. Mol. Med. *14*, 357–367.

Callender, L.A., Carroll, E.C., Beal, R.W.J., Chambers, E.S., Nourshargh, S., Akbar, A.N., and Henson, S.M. (2018). Human $CD8^+$ EMRA T cells display a senescence-associated secretory phenotype regulated by p38 MAPK. Aging Cell *17*, e12675.

Chen, H.P., Li, L., Chen, X., Yang, M.F., Ye, Y., Wang, X.Q., and Xu, Y. (2017). The mechanism of Jurkat cells apoptosis induced by Aggregatibacter actinomycetemcomitans cytolethal distending toxin. Apoptosis *22*, 841–851.

Chou, J.P., and Effros, R.B. (2013). T cell replicative senescence in human aging. Curr. Pharm. Des. *19*, 1680–1698.

Chumduri, C., Gurumurthy, R.K., Zietlow, R., and Meyer, T.F. (2016). Subversion of host genome integrity by bacterial pathogens. Nat. Rev. Mol. Cell Biol. *17*, 659–673.

Coppé, J.P., Patil, C.K., Rodier, F., Sun, Y., Muñoz, D.P., Goldstein, J., Nelson, P.S., Desprez, P.Y., and Campisi, J. (2008). Senescence-associated secretory phenotypes reveal cell-nonautonomous functions of oncogenic RAS and the p53 tumor suppressor. PLoS Biol. *6*, 2853–2868.

Cougnoux, A., Dalmasso, G., Martinez, R., Buc, E., Delmas, J., Gibold, L., Sauvanet, P., Darcha, C., Déchelotte, P., Bonnet, M., et al. (2014). Bacterial genotoxin colibactin promotes colon tumour growth by inducing a senescence-associated secretory phenotype. Gut *63*, 1932–1942.

Covre, L.P., Martins, R.F., Devine, O.P., Chambers, E.S., Vukmanovic-Stejic, M., Silva, J.A., Dietze, R., Rodrigues, R.R., de Matos Guedes, H.L., Falqueto, A., et al. (2019). Circulating Senescent T Cells Are Linked to Systemic Inflammation and Lesion Size During Human Cutaneous Leishmaniasis. Front. Immunol. *9*, 3001.

Del Bel Belluz, L., Guidi, R., Pateras, I.S., Levi, L., Mihaljevic, B., Rouf, S.F., Wrande, M., Candela, M., Turroni, S., Nastasi, C., et al. (2016). The Typhoid Toxin Promotes Host Survival and the Establishment of a Persistent Asymptomatic Infection. PLoS Pathog. *12*, e1005528.

Di Mitri, D., Azevedo, R.I., Henson, S.M., Libri, V., Riddell, N.E., Macaulay, R., Kipling, D., Soares, M.V., Battistini, L., and Akbar, A.N. (2011). Reversible senescence in human CD4+CD45RA+CD27- memory T cells. J. Immunol. *187*, 2093–2100.

DiRienzo, J.M. (2014). Uptake and processing of the cytolethal distending toxin by mammalian cells. Toxins (Basel) *6*, 3098–3116.

Dixon, S.D., Huynh, M.M., Tamilselvam, B., Spiegelman, L.M., Son, S.B., Eshraghi, A., Blanke, S.R., and Bradley, K.A. (2015). Distinct Roles for CdtA and CdtC during Intoxication by Cytolethal Distending Toxins. PLoS ONE *10*, e0143977.

Dlakic, M. (2001). Is CdtB a nuclease or a phosphatase? Science *291*, 547.

Evangelou, K., Lougiakis, N., Rizou, S.V., Kotsinas, A., Kletsas, D., Muñoz-Espín, D., Kastrinakis, N.G., Pouli, N., Marakos, P., Townsend, P., et al. (2017). Robust, universal biomarker assay to detect senescent cells in biological specimens. Aging Cell *16*, 192–197.

Fahrer, J., Huelsenbeck, J., Jaurich, H., Dörsam, B., Frisan, T., Eich, M., Roos, W.P., Kaina, B., and Fritz, G. (2014). Cytolethal distending toxin (CDT) is a radiomimetic agent and induces persistent levels of DNA double-strand breaks in human fibroblasts. DNA Repair (Amst.) *18*, 31–43.

Faïs, T., Delmas, J., Serres, A., Bonnet, R., and Dalmasso, G. (2016). Impact of CDT Toxin on Human Diseases. Toxins (Basel) *8*, 220.

Fedor, Y., Vignard, J., Nicolau-Travers, M.L., Boutet-Robinet, E., Watrin, C., Salles, B., and Mirey, G. (2013). From single-strand breaks to double-strand breaks during S-phase: a new mode of action of the Escherichia coli Cytolethal Distending Toxin. Cell. Microbiol. *15*, 1–15.

Fox, J.G., Rogers, A.B., Whary, M.T., Ge, Z., Taylor, N.S., Xu, S., Horwitz, B.H., and Erdman, S.E. (2004). Gastroenteritis in NF-kappaB-deficient mice is produced with wild-type Camplyobacter jejuni but not with C. jejuni lacking cytolethal distending toxin despite persistent colonization with both strains. Infect. Immun. *72*, 1116–1125.

Freund, A., Patil, C.K., and Campisi, J. (2011). p38MAPK is a novel DNA damage response-independent regulator of the senescence-associated secretory phenotype. EMBO J. *30*, 1536–1548.

Freund, A., Laberge, R.M., Demaria, M., and Campisi, J. (2012). Lamin B1 loss is a senescence-associated biomarker. Mol. Biol. Cell *23*, 2066–2075.

Gagnaire, A., Nadel, B., Raoult, D., Neefjes, J., and Gorvel, J.P. (2017). Collateral damage: insights into bacterial mechanisms that predispose host cells to cancer. Nat. Rev. Microbiol. *15*, 109–128.

Gargi, A., Reno, M., and Blanke, S.R. (2012). Bacterial toxin modulation of the eukaryotic cell cycle: are all cytolethal distending toxins created equally? Front. Cell. Infect. Microbiol. *2*, 124.

Ge, Z., Schauer, D.B., and Fox, J.G. (2008). In vivo virulence properties of bacterial cytolethal-distending toxin. Cell. Microbiol. *10*, 1599–1607.

Georgakopoulou, E.A., Tsimaratou, K., Evangelou, K., Fernandez Marcos, P.J., Zoumpourlis, V., Trougakos, I.P., Kletsas, D., Bartek, J., Serrano, M., and Gorgoulis, V.G. (2013). Specific lipofuscin staining as a novel biomarker to detect replicative and stress-induced senescence. A method applicable in cryo-preserved and archival tissues. Aging (Albany NY) *5*, 37–50.

Gorgoulis, V., Adams, P.D., Alimonti, A., Bennett, D.C., Bischof, O., Bishop, C., Campisi, J., Collado, M., Evangelou, K., Ferbeyre, G., et al. (2019). Cellular Senescence: Defining a Path Forward. Cell *179*, 813–827.

Grasso, F., and Frisan, T. (2015). Bacterial Genotoxins: Merging the DNA Damage Response into Infection Biology. Biomolecules *5*, 1762–1782.

Guerra, L., Teter, K., Lilley, B.N., Stenerlöw, B., Holmes, R.K., Ploegh, H.L., Sandvig, K., Thelestam, M., and Frisan, T. (2005). Cellular internalization of cytolethal distending toxin: a new end to a known pathway. Cell. Microbiol. *7*, 921–934.

Guerra, L., Carr, H.S., Richter-Dahlfors, A., Masucci, M.G., Thelestam, M., Frost, J.A., and Frisan, T. (2008). A bacterial cytotoxin identifies the RhoA

exchange factor Net1 as a key effector in the response to DNA damage. PLoS ONE *3*, e2254.

Guerra, L., Guidi, R., and Frisan, T. (2011a). Do bacterial genotoxins contribute to chronic inflammation, genomic instability and tumor progression? FEBS J. *278*, 4577–4588.

Guerra, L., Guidi, R., Slot, I., Callegari, S., Sompallae, R., Pickett, C.L., Åström, S., Eisele, F., Wolf, D., Sjögren, C., et al. (2011b). Bacterial genotoxin triggers FEN1-dependent RhoA activation, cytoskeleton remodeling and cell survival. J. Cell Sci. *124*, 2735–2742.

Ibler, A.E.M., ElGhazaly, M., Naylor, K.L., Bulgakova, N.A., F El-Khamisy, S., and Humphreys, D. (2019). Typhoid toxin exhausts the RPA response to DNA replication stress driving senescence and Salmonella infection. Nat. Commun. *10*, 4040.

Jinadasa, R.N., Bloom, S.E., Weiss, R.S., and Duhamel, G.E. (2011). Cytolethal distending toxin: a conserved bacterial genotoxin that blocks cell cycle progression, leading to apoptosis of a broad range of mammalian cell lineages. Microbiology (Reading) *157*, 1851–1875.

Jorgensen, I., Rayamajhi, M., and Miao, E.A. (2017). Programmed cell death as a defence against infection. Nat. Rev. Immunol. *17*, 151–164.

Kang, C., Xu, Q., Martin, T.D., Li, M.Z., Demaria, M., Aron, L., Lu, T., Yankner, B.A., Campisi, J., and Elledge, S.J. (2015). The DNA damage response induces inflammation and senescence by inhibiting autophagy of GATA4. Science *349*, aaa5612.

Kim, H.J., Cho, J.H., Quan, H., and Kim, J.R. (2011). Down-regulation of Aurora B kinase induces cellular senescence in human fibroblasts and endothelial cells through a p53-dependent pathway. FEBS Lett. *585*, 3569–3576.

Kosar, M., Bartkova, J., Hubackova, S., Hodny, Z., Lukas, J., and Bartek, J. (2011). Senescence-associated heterochromatin foci are dispensable for cellular senescence, occur in a cell type- and insult-dependent manner and follow expression of p16(ink4a). Cell Cycle *10*, 457–468.

Krejsgaard, T., Vetter-Kauczok, C.S., Woetmann, A., Lovato, P., Labuda, T., Eriksen, K.W., Zhang, Q., Becker, J.C., and Ødum, N. (2006). Jak3- and JNK-dependent vascular endothelial growth factor expression in cutaneous T-cell lymphoma. Leukemia *20*, 1759–1766.

Kuwahara, M., Suzuki, J., Tofukuji, S., Yamada, T., Kanoh, M., Matsumoto, A., Maruyama, S., Kometani, K., Kurosaki, T., Ohara, O., et al. (2014). The Menin-Bach2 axis is critical for regulating CD4 T-cell senescence and cytokine homeostasis. Nat. Commun. *5*, 3555.

Lanna, A., Henson, S.M., Escors, D., and Akbar, A.N. (2014). The kinase p38 activated by the metabolic regulator AMPK and scaffold TAB1 drives the senescence of human T cells. Nat. Immunol. *15*, 965–972.

Lara-Tejero, M., and Galán, J.E. (2000). A bacterial toxin that controls cell cycle progression as a deoxyribonuclease I-like protein. Science *290*, 354–357.

Macaulay, R., Akbar, A.N., and Henson, S.M. (2013). The role of the T cell in age-related inflammation. Age (Dordr.) *35*, 563–572.

Martin, O.C.B., and Frisan, T. (2020). Bacterial Genotoxin-Induced DNA Damage and Modulation of the Host Immune Microenvironment. Toxins (Basel) *12*, 63.

McAuley, J.L., Linden, S.K., Png, C.W., King, R.M., Pennington, H.L., Gendler, S.J., Florin, T.H., Hill, G.R., Korolik, V., and McGuckin, M.A. (2007). MUC1 cell surface mucin is a critical element of the mucosal barrier to infection. J. Clin. Invest. *117*, 2313–2324.

Nesić, D., Hsu, Y., and Stebbins, C.E. (2004). Assembly and function of a bacterial genotoxin. Nature *429*, 429–433.

Ohara, M., Hayashi, T., Kusunoki, Y., Miyauchi, M., Takata, T., and Sugai, M. (2004). Caspase-2 and caspase-7 are involved in cytolethal distending toxin-induced apoptosis in Jurkat and MOLT-4 T-cell lines. Infect. Immun. *72*, 871–879.

Ohara, M., Hayashi, T., Kusunoki, Y., Nakachi, K., Fujiwara, T., Komatsuzawa, H., and Sugai, M. (2008). Cytolethal distending toxin induces caspase-dependent and -independent cell death in MOLT-4 cells. Infect. Immun. *76*, 4783–4791.

Pateras, I.S., Havaki, S., Nikitopoulou, X., Vougas, K., Townsend, P.A., Panayiotidis, M.I., Georgakilas, A.G., and Gorgoulis, V.G. (2015). The DNA damage response and immune signaling alliance: Is it good or bad? Nature decides when and where. Pharmacol. Ther. *154*, 36–56.

Rodier, F., Coppé, J.P., Patil, C.K., Hoeijmakers, W.A., Muñoz, D.P., Raza, S.R., Freund, A., Campeau, E., Davalos, A.R., and Campisi, J. (2009). Persistent DNA damage signalling triggers senescence-associated inflammatory cytokine secretion. Nat. Cell Biol. *11*, 973–979.

Scuron, M.D., Boesze-Battaglia, K., Dlakić, M., and Shenker, B.J. (2016). The Cytolethal Distending Toxin Contributes to Microbial Virulence and Disease Pathogenesis by Acting As a Tri-Perditious Toxin. Front. Cell. Infect. Microbiol. *6*, 168.

Secher, T., Samba-Louaka, A., Oswald, E., and Nougayrède, J.P. (2013). Escherichia coli producing colibactin triggers premature and transmissible senescence in mammalian cells. PLoS ONE *8*, e77157.

Sharpless, N.E., and Sherr, C.J. (2015). Forging a signature of in vivo senescence. Nat. Rev. Cancer *15*, 397–408.

Shen, Z., Feng, Y., Rogers, A.B., Rickman, B., Whary, M.T., Xu, S., Clapp, K.M., Boutin, S.R., and Fox, J.G. (2009). Cytolethal distending toxin promotes Helicobacter cinaedi-associated typhlocolitis in interleukin-10-deficient mice. Infect. Immun. *77*, 2508–2516.

Shenker, B.J., McKay, T., Datar, S., Miller, M., Chowhan, R., and Demuth, D. (1999). Actinobacillus actinomycetemcomitans immunosuppressive protein is a member of the family of cytolethal distending toxins capable of causing a G2 arrest in human T cells. J. Immunol. *162*, 4773–4780.

Shenker, B.J., Hoffmaster, R.H., McKay, T.L., and Demuth, D.R. (2000). Expression of the cytolethal distending toxin (Cdt) operon in Actinobacillus actinomycetemcomitans: evidence that the CdtB protein is responsible for G2 arrest of the cell cycle in human T cells. J. Immunol. *165*, 2612–2618.

Shenker, B.J., Hoffmaster, R.H., Zekavat, A., Yamaguchi, N., Lally, E.T., and Demuth, D.R. (2001). Induction of apoptosis in human T cells by Actinobacillus actinomycetemcomitans cytolethal distending toxin is a consequence of G2 arrest of the cell cycle. J. Immunol. *167*, 435–441.

Shenker, B.J., Demuth, D.R., and Zekavat, A. (2006). Exposure of lymphocytes to high doses of Actinobacillus actinomycetemcomitans cytolethal distending toxin induces rapid onset of apoptosis-mediated DNA fragmentation. Infect. Immun. *74*, 2080–2092.

Shenker, B.J., Dlakic, M., Walker, L.P., Besack, D., Jaffe, E., LaBelle, E., and Boesze-Battaglia, K. (2007). A novel mode of action for a microbial-derived immunotoxin: the cytolethal distending toxin subunit B exhibits phosphatidylinositol 3,4,5-triphosphate phosphatase activity. J. Immunol. *178*, 5099–5108.

Taieb, F., Petit, C., Nougayrède, J.P., and Oswald, E. (2016). The Enterobacterial Genotoxins: Cytolethal Distending Toxin and Colibactin. Ecosal Plus *7*.

Tchkonia, T., Zhu, Y., van Deursen, J., Campisi, J., and Kirkland, J.L. (2013). Cellular senescence and the senescent secretory phenotype: therapeutic opportunities. J. Clin. Invest. *123*, 966–972.

Toledo, L.I., Murga, M., Gutierrez-Martinez, P., Soria, R., and Fernandez-Capetillo, O. (2008). ATR signaling can drive cells into senescence in the absence of DNA breaks. Genes Dev. *22*, 297–302.

Tuffs, S.W., Haeryfar, S.M.M., and McCormick, J.K. (2018). Manipulation of Innate and Adaptive Immunity by Staphylococcal Superantigens. Pathogens *7*, E53.

van Deursen, J.M. (2014). The role of senescent cells in ageing. Nature *509*, 439–446.

von Essen, M., Nielsen, M.W., Bonefeld, C.M., Boding, L., Larsen, J.M., Leitges, M., Baier, G., Odum, N., and Geisler, C. (2006). Protein kinase C (PKC) alpha and PKC theta are the major PKC isotypes involved in TCR down-regulation. J. Immunol. *176*, 7502–7510.

Wising, C., Azem, J., Zetterberg, M., Svensson, L.A., Ahlman, K., and Lagergård, T. (2005a). Induction of apoptosis/necrosis in various human cell

lineages by Haemophilus ducreyi cytolethal distending toxin. Toxicon *45*, 767–776.

Wising, C., Mölne, L., Jonsson, I.M., Ahlman, K., and Lagergård, T. (2005b). The cytolethal distending toxin of Haemophilus ducreyi aggravates dermal lesions in a rabbit model of chancroid. Microbes Infect. *7*, 867–874.

Xu, W., and Larbi, A. (2017). Markers of T Cell Senescence in Humans. Int. J. Mol. Sci. *18*, 1742.

Yi, H.S., Kim, S.Y., Kim, J.T., Lee, Y.S., Moon, J.S., Kim, M., Kang, Y.E., Joung, K.H., Lee, J.H., Kim, H.J., et al. (2019). T-cell senescence contributes to abnormal glucose homeostasis in humans and mice. Cell Death Dis. *10*, 249.

Zhang, B., Fu, D., Xu, Q., Cong, X., Wu, C., Zhong, X., Ma, Y., Lv, Z., Chen, F., Han, L., et al. (2018). The senescence-associated secretory phenotype is potentiated by feedforward regulatory mechanisms involving Zscan4 and TAK1. Nat. Commun. *9*, 1723.

## STAR★METHODS

### KEY RESOURCES TABLE

| REAGENT or RESOURCE | SOURCE | IDENTIFIER |
|---|---|---|
| **Antibodies** | | |
| Rabbit monoclonal anti-phospho-ATM (Ser1981), western blotting | Cell Signaling Technology | Cat#5883; RRID:AB_10835213 |
| Rabbit monoclonal anti-ATM, western blotting | Cell Signaling Technology | Cat#2873; RRID:AB_2062659 |
| Rabbit monoclonal anti-phospho-H2AX (Ser139), western blotting | Cell Signaling Technology | Cat#9718; RRID:AB_2118009 |
| Rabbit monoclonal anti-H2AX, western blotting | Cell Signaling Technology | Cat#7631; RRID:AB_10860771 |
| Goat polyclonal anti-p16$^{INK4A}$, western blotting | R&D systems | Cat#AF5779; RRID:AB_1964666 |
| Rabbit monoclonal anti-p21$^{WAF1/CIP1}$, western blotting | Cell Signaling Technology | Cat#2947; RRID:AB_823586 |
| Rabbit monoclonal anti-phospho-p38 MAPK (Thr180/Tyr182), western blotting | Cell Signaling Technology | Cat#9215; RRID:AB_331762 |
| Rabbit polyclonal anti-p38 MAPK, western blotting | Cell Signaling Technology | Cat#9212; RRID:AB_330713 |
| Mouse monoclonal anti-phospho-p53 (Ser15), western blotting | Cell Signaling Technology | Cat#9286; RRID:AB_331741 |
| Mouse monoclonal anti-p53, western blotting | Cell Signaling Technology | Cat#2524; RRID:AB_331743 |
| Mouse monoclonal anti-GAPDH, western blotting | Santa Cruz Biotechnology | Cat#sc-365062; RRID:AB_10847862 |
| Mouse monoclonal anti-p21$^{WAF1/CIP1}$, immunocytochemistry | Santa Cruz Biotechnology | Cat#sc-6246; RRID:AB_628073 |
| Rabbit polyclonal phospho-p38 MAPK (Thr180/Tyr182), immunocytochemistry | Cell Signaling Technology | Cat#9211; RRID:AB_331641 |
| Rabbit polyclonal anti-CD3, immunocytochemistry | Abcam | Cat#ab5690; RRID:AB_305055 |
| Mouse monoclonal anti-p16, immunocytochemistry | Roche | Cat#6695248001; RRID:AB_2833232 |
| Mouse monoclonal anti-CD45RA-PE/Cy7, flow cytometry | BioLegend | Cat#304126; RRID:AB_10708879 |
| Mouse monoclonal anti-CD27-APC, flow cytometry | BioLegend | Cat#356410; RRID:AB_2561957 |
| Mouse monoclonal anti-CD45RO-APC/Cy7, flow cytometry | BioLegend | Cat#304228; RRID:AB_1089589 |
| **Bacterial and virus strains** | | |
| *S*. Typhimurium strain MC1-TT | Prof. Teresa Frisan | Del Bel Belluz et al., 2016 |
| *S*. Typhimurium strain MC1-ΔcdtB | Prof. Teresa Frisan | Del Bel Belluz et al., 2016 |
| **Biological samples** | | |
| Buffy coats | Danish Blood Bank | N/A |
| **Chemicals, peptides, and recombinant proteins** | | |
| CDT | This paper | N/A |
| GL13 (SenTraGor®) | Arriani Pharmaceuticals | Cat#AR88500040; Lot#170701 |
| SB203580 | Sigma-Aldrich | Cat#S8307; CAS: 152121-47-6 |
| KU60019 | Selleck Chemicals | Cat#S1570; CAS: 925701-49-1 |
| 7-AAD | Sigma-Aldrich | Cat#A9400; CAS: 7240-37-1 |
| **Critical commercial assays** | | |
| Naive CD4+ T Cell Isolation Kit II, human | Miltenyi Biotec | Cat#130-094-131 |
| CD4+ Effector Memory T Cell Isolation Kit, human | Miltenyi Biotec | Cat#130-094-125 |
| X-VIVO 15 Serum-Free Hematopoietic Cell Medium | Lonza | Cat#BE02-060F |
| Dynabeads Human T-activator CD3/CD28 | Thermo Fisher Scientific | Cat#11131D |
| CellTrace Violet Cell Proliferation Kit | Thermo Fisher Scientific | Cat#C34557 |
| Trypan Blue Dye 0.40% | Bio-Rad | Cat#1450021 |

(*Continued on next page*)

*Continued*

| REAGENT or RESOURCE | SOURCE | IDENTIFIER |
|---|---|---|
| 7-AAD Viability Staining Solution | BioLegend | Cat#420404 |
| Human IL-17 DuoSet ELISA | R&D systems | Cat#DY317 |
| Human IL-13 DuoSet ELISA | R&D systems | Cat#DY213 |
| Human IFNγ DuoSet ELISA | R&D systems | Cat#DY285B |
| Human CCL1/I-309 DuoSet ELISA | R&D systems | Cat#DY272 |
| Human IL-3 DuoSet ELISA | R&D systems | Cat#DY203 |
| Human IL-5 DuoSet ELISA | R&D systems | Cat#DY205 |
| Human GM-CSF DuoSet ELISA | R&D systems | Cat#DY215 |
| Human IL-6 DuoSet ELISA | R&D systems | Cat#DY206 |
| Human IL-8/CXCL8 DuoSet ELISA | R&D systems | Cat#DY208 |
| Human IL-10 DuoSet ELISA | R&D systems | Cat#DY217B |
| Human IL-22 DuoSet ELISA | R&D systems | Cat#DY782 |
| Human IL-21 Uncoated ELISA | Invitrogen | Cat#88-8218 |
| IL-9 Human ELISA MAX Deluxe | BioLegend | Cat#434704 |
| Bio-Rad Protein Assay Dye Reagent Concentrate | Bio-Rad | Cat#5000006EDU |
| Amersham ECL Prime Western Blotting Detection Reagent | Sigma-Aldrich | Cat#RPN2236 |
| UltraVision LP Detection System | Thermo Fisher Scientific | Cat#TL-060-HD |
| TripleStain IHC Kit | Abcam | Cat#ab183286 |
| RNeasy Plus Mini Kit | QIAGEN | Cat#74136 |
| Applied Biosystems High-Capacity cDNA Reverse Transcription Kit | Thermo Fisher Scientific | Cat#4368814 |
| LightCycler 480 Probes Master | Roche | Cat#4887301001 |
| Applied Biosystems pre-designed human TaqMan Gene Expression Assays | Thermo Fisher Scientific | Table S1 |
| Power SYBR® Green PCR Master Mix | Thermo Fisher Scientific | Cat#4368577 |
| Primers used for murine cDNA samples | This paper | Table S2 |
| Experimental models: Cell lines | | |
| Jurkat T cell line | Prof. Carsten Geisler | von Essen et al., 2006; RRID:CVCL_C831 |
| Experimental models: Organisms/strains | | |
| Sv129 mice | Taconic Biosciences | 129SVE-F |
| Recombinant DNA | | |
| Expression vectors encoding CdtA, CdtB, CdtB$^{D273R}$, and CdtC | Prof. Teresa Frisan | Guerra et al., 2005, 2011b |
| Software and algorithms | | |
| FlowJo v10 software | Tree Star | RRID:SCR_008520 |
| LightCycler 480 SW 1.5.1 software | Roche | Cat#4994884001 |
| Image Lab software | Bio-Rad | Cat#1709690 |
| GraphPad Prism 7 software | GraphPad | RRID:SCR_002798 |

## RESOURCE AVAILABILITY

### Lead contact

Further information and requests for resources and reagents should be directed to and will be fulfilled by the Lead Contact, Thorbjørn Krejsgaard (thorkr@sund.ku.dk).

### Materials availability

This study did not generate any new unique reagents. CDT is available upon request.

### Data and code availability

This study did not generate any unique datasets or code.

## EXPERIMENTAL MODEL AND SUBJECT DETAILS

### Mice

Female Sv129 mice 6 to 8 weeks old were obtained from Taconic Biosciences Inc. (Bomholt, Denmark) and housed in a pathogen-free facility. The *S*. Typhimurium strains MC1-TT and MC1-ΔcdtB were generated and described previously (Del Bel Belluz et al., 2016). These strains were employed to infect Sv129 mice as described in Del Bel Belluz et al. (2016). 10 days post infection the small intestines were collected and subjected to further analysis. Mice were handled according to good animal practice based on national animal welfare bodies and strictly following proceedings in EU legislation. The study was approved by the Regional Animal Studies Ethical Committee Northern Norrland, Sweden (reference number A17-17).

### Primary human CD4 T cells

PBMCs were isolated by Lymphoprep (STEMCELL Technologies, Cambridge, UK) density gradient centrifugation from buffy coats that were obtained from healthy blood donors at the Danish Blood Bank (Department of Clinical Immunology, University Hospital Rigshospitalet, Copenhagen, Denmark) with informed consent. In accordance with Danish legislation and ethical guidelines, the buffy coats were only identified by date of blood sampling and analyzed completely anonymously without the possibility to obtain any donor-specific information. Human naive CD4+ T cells (Tn) and CD4+ effector memory T cells (Tem) were subsequently isolated from freshly purified PBMCs by negative selection using the human Naive CD4+ T Cell Isolation Kit II and the human CD4+ Effector Memory T Cell Isolation Kit, respectively, from Miltenyi Biotec (Bergisch Gladbach, Germany) in accordance with the manufacturers' instructions. The purified T cells were cultured at 37°C and 5% $CO_2$ in serum-free X-VIVO 15 medium (Lonza, Basel, Switzerland) in flat-bottom 24-well or 96-well tissue culture plates with or without Dynabeads Human T-activator CD3/CD28 (αCD3/CD28 beads) (Thermo Fisher Scientific, Waltham, MA, USA) and CDT. After culture, the αCD3/CD28 beads were removed by magnetic depletion prior to further analysis. The p38 inhibitor, SB203580 (Sigma-Aldrich, ST. Louis, MO, USA), and the ATM inhibitor, KU60019 (Selleck Chemicals, Munich, Germany), were dissolved in dimethyl sulfoxide (DMSO) (Sigma-Aldrich) and added to the cell cultures in some experiments as given. In these experiments, an equal concentration of DMSO without inhibitor was added to cultures as vehicle control.

### Jurkat T cell line

The human Jurkat T cell line (von Essen et al., 2006) was cultured in RPMI 1640 AQmedia (Sigma-Aldrich) with 10% fetal bovine serum (FBS) (Biological Industries, Cromwell, CT, USA) and 100μg/mL pencillin/streptomycin (Sigma-Aldrich) at 37°C and 5% $CO_2$.

## METHOD DETAILS

### Recombinant CDT and mCDT

Expression vectors encoding recombinant CdtA, CdtB, $CdtB^{D273R}$, and CdtC subunits cloned from *H. ducreyi* were constructed previously (Guerra et al., 2005, 2011b). The recombinant CDT subunits were overexpressed as His-tagged proteins in *E. coli* BL21. The CDT subunits were purified from inclusion bodies under denaturing conditions using Ni-NTA affinity chromatography and dialyzed in refolding buffer (100mM Tris-HCl pH 7.5, 400mM L-Arginine, 20% Glycerol, 7M Urea). Urea was gradually removed during dialysis to provide gradual refolding of the CDT subunits. Finally, the active CDT (CdtA, CdtB, and CdtC) and mCDT (CdtA, $CdtB^{D273R}$, and CdtC) holotoxins were reconstituted by incubating equal moles of each purified subunit together for 30 min. at 37°C.

### Cell counting

Cells were stained with 0.40% Trypan Blue Dye (Bio-Rad, Hercules, CA, USA) and the concentration of live cells counted using a TC20TM Automated Cell Counter (Bio-Rad). Each sample was counted three times and the average value calculated.

### Enzyme-Linked Immunosorbent Assay

The concentrations of IL-3, IL-5, IL-6, IL-8, IL-10, IL-13, IL-17, IL-22, IFNγ, CSF2, and CCL1 in cell culture supernatants were measured using human DuoSet Enzyme-Linked Immunosorbent Assay (ELISA) kits from R&D systems (Minneapolis, MN, USA). The concentrations of IL-9 and IL-21 in cell culture supernatants were measured using IL-9 Human ELISA MAX Deluxe set (BioLegend, San Diego, CA, USA) and IL-21 Human uncoated ELISA kit (Invitrogen, Carlsbad, CA, USA), respectively.

### QPCR analysis

Total RNA was purified from cell pellets or mouse tissue using the RNeasy Plus Mini Kit from QIAGEN (Germantown, MD, USA) with depletion of genomic DNA by gDNA Eliminator spin columns. The purified RNA was reverse transcribed into complementary DNA (cDNA) using the Applied Biosystems High Capacity cDNA Reverse Transcription Kit (Thermo Fisher Scientific). For human samples, the cDNA was mixed with LightCycler 480 Probes Master (Roche, Basel, Switzerland) and Applied Biosystems pre-designed human

TaqMan Gene Expression Assay (Thermo Fisher Scientific) containing specific primers and a FAM-labeled probe against the gene of interest. The reaction mixtures were amplified in a LightCycler® 480 Instrument II (Roche) and Cp values obtained using LightCycler® 480 SW 1.5.1 Software. For mouse samples, the cDNA was mixed with Power SYBR® Green PCR Master Mix (Thermo Scientific) and primers against the gene of interest. The reaction mixture was amplified in a ABI PRISM® 7000 Sequence Detection System (Applied Biosystems). The pre-designed Human Taqman Gene Expression Assays used in the study are listed in Table S1 and the primers used for murine cDNA samples are listed in Table S2. The relative gene expression (Rel. expression) or fold change was calculated using the $2^{-\Delta Cp}$ or $2^{-\Delta\Delta Cp}$ method, respectively, with *GAPDH* as reference gene.

### Western blotting

Cellular protein extraction and western blotting were performed as described earlier (Krejsgaard et al., 2006). The total protein concentrations of the cellular lysates were determined by Bio-Rad Protein Assay (Bio-Rad) and equal amounts (μg) of each sample analyzed. Amersham ECL Prime Western Blotting Detection Reagent (Sigma-Aldrich) was used for detection. Chemiluminescence was captured using the ChemiDOC™ XRS+ system (Bio-Rad) and the data analyzed using Image Lab 4.0 software (Bio-Rad).

### Flow cytometry

For analysis of cell cycle distribution based on cellular DNA contents, cells were incubated in saponin buffer (0.03% saponin in phosphate-buffered saline (PBS)) containing 4 ug/mL 7-aminoactinomycin D (7-AAD) (Sigma-Aldrich) for 30 min. at room temperature (RT) before flow cytometric acquisition. For viability analysis, the cells were resuspended in Annexin V Binding Buffer (BioLegend) and stained for 15 min with fluorochrome-conjugated Annexin V (BioLegend) at 4°C in the dark. Then, the cells were washed, 7-AAD Viability Staining Solution (BioLegend) added, and the cells subjected to flow cytometric acquisition. For analysis of CD45RA and CD27 cell surface expression, cells were stained with PE/Cy7-conjugated anti-CD45RA (clone HI100 from BioLegend) and APC conjugated anti-CD27 (clone M-T271 from BioLegend) antibodies in ice-cold FACS buffer (1% FBS and 0.02% Na-azide in PBS) for 30 min. at 4°C protected from light prior flow cytometric acquisition. To track cell division, freshly purified Tn or Tem cells were washed with staining buffer (1% FBS in PBS) and incubated for 5 min. at RT with staining buffer containing 5μM CellTrace Violet (Thermo Fisher Scientific). The staining was subsequently terminated by addition of 10% FBS in RPMI-1640 medium and the cells washed in X-VIVO 15 media before they were cultured with or without Human T-activator CD3/CD28 Dynabeads and CDT as described above. After culture, the cells were stained with APC/Cy7-conjugated CD45RO (clone UCHL1, BioLegend) in ice-cold FACS buffer for 30 min. at 4°C protected from light and subjected to flow cytometric acquisition. Flow cytometric acquisition was performed at the Core Facility for Flow Cytometry (Faculty of Health and Medical Sciences, University of Copenhagen) using Fortessa 3 and 5 flow cytometers (BD Biosciences, Franklin Lakes, NJ, USA). The acquired data were analyzed with FlowJo v10 software (Tree Star, Ashland, OR, USA). Except in the analysis of cell cycle distribution, 7-AAD Viability Staining Solution was added to the cell samples shortly before acquisition and dead cells (7-AAD+) excluded in the data analysis.

### Immunocytochemistry and immunohistochemistry

For immunocytochemistry, the cells were washed in PBS and incubated for 30 min. at RT with 10% neutral buffered formalin (CellPath, Newtown, UK). After further washing, the fixed cells were stained with hematoxylin (Sigma-Aldrich) and embedded in 2% Agarose (Sigma-Aldrich). The resulting agarose blocks were subsequently embedded in paraffin. For the immunocytochemical stainings, we utilized the UltraVision LP Detection System (#TL-060-HD, Thermo Scientific) according to the manufacturer's instructions. The following antibodies were used: anti-p21 (F-5, sc-6246, Santa Cruz Biotechnology), anti-p16 (E6H4, 6695248001, Roche) and anti-p-p38 (9211, Cell Signaling Technology). Both for p21, p16, and p-p38, we counted the percentage of T cells exhibiting intense nuclear staining. Evaluation of senescence was performed employing a hybrid histo-/immuno chemical assay utilizing GL13 (commercially available as SenTraGor®), a lipophilic, biotin-linked Sudan Black-B (SBB) analog (Evangelou et al., 2017). For immunohistochemistry, the small intestines from infected and uninfected mice were collected and processed as previously described (Del Bel Belluz et al., 2016). To perform the CD3/GL13 staining, we employed the TripleStain IHC Kit (ab183286) from Abcam (Cambridge, UK) following the manufacturer's instructions. Specifically, we proceeded to sequential CD3 (ab5690, Abcam) immunostaining visualized with DAB chromogen (brown color) and GL13 staining visualized with emerald color. The evaluation was performed by counting in the stroma the (CD3+GL13+)/(CD3+) ratio per high power field (magnification 400x). Mouse spleen served as positive control for CD3. Previously characterized cases were employed as positive control for GL13 (Evangelou et al., 2017). Hematoxylin and Eosin (H-E) staining was performed to assess severity of enteritis.

## QUANTIFICATION AND STATISTICAL ANALYSIS

Statistical analyses were performed using GraphPad Prism 7.00 software. Untransformed ΔCp values ($Cp_{TARGET\ GENE} - Cp_{REFERENCE\ GENE}$) were employed for statistical analysis of QPCR experiments and *GAPDH* used as reference gene. Likewise, untransformed cytokine concentrations were used for the statistical analysis of ELISA data. Statistical significance was defined as a p value below 0.05, and *n* represents the number of analyzed donors. All the statistical details of experiments (including the statistical tests used, exact value of *n*, definition of center, dispersion and precision measures) can be found in the figure legends.

**Cell Reports, Volume *35***

## Supplemental information

# Bacterial genotoxins induce T cell senescence

**Sarah L. Mathiasen, Laura Gall-Mas, Ioannis S. Pateras, Sofia D.P. Theodorou, Martin R.J. Namini, Morten B. Hansen, Océane C.B. Martin, Chella Krishna Vadivel, Konstantinos Ntostoglou, Deborah Butter, Michael Givskov, Carsten Geisler, Arne N. Akbar, Vassilis G. Gorgoulis, Teresa Frisan, Niels Ødum, and Thorbjørn Krejsgaard**

## SUPPLEMENTAL INFORMATION

**Figure S1.** The catalytic activity of CDT promotes secretion of signature effector cytokines from activated, but not resting, CD4 T cells. Related to Figure 1.

**Figure S2.** Jurkat T cells and activated primary CD4 T cells respond differently to CDT intoxication. Related to Figure 2.

**Figure S3.** CDT promotes phenotypic traits of senescence in activated CD4 T cells. Related to Figure 3.

**Figure S4.** CDT-induced T cell senescence is not dependent on activation of the ATM-p38 axis. Related to Figure 4.

**Table S1.** Applied Biosystems pre-designed human TaqMan Gene Expression Assays used in the study. Related to STAR methods.

**Table S2.** Primers used for SYBR green QPCR analyses of murine samples. Related to STAR methods.

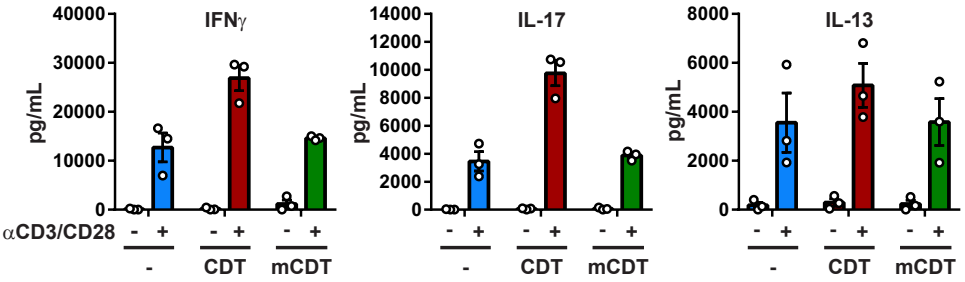


**Figure S1. The catalytic activity of CDT promotes secretion of signature effector cytokines from activated, but not resting, CD4 T cells. Related to Figure 1.** Effector memory CD4 T cells were cultured for 5 days in absence (-) or presence of αCD3/CD28 beads, 200 ng/mL CDT or 200ng/mL of a catalytically inactive form of CDT (mCDT) harboring a mutation (D273R) in the magnesium-binding site of CdtB. Subsequently, the concentrations of IFNγ, IL-17, and IL-13 were measured in the cell culture supernatants by ELISA. Circles represent individual donors and bars the mean ± SEM (*n* = 3).

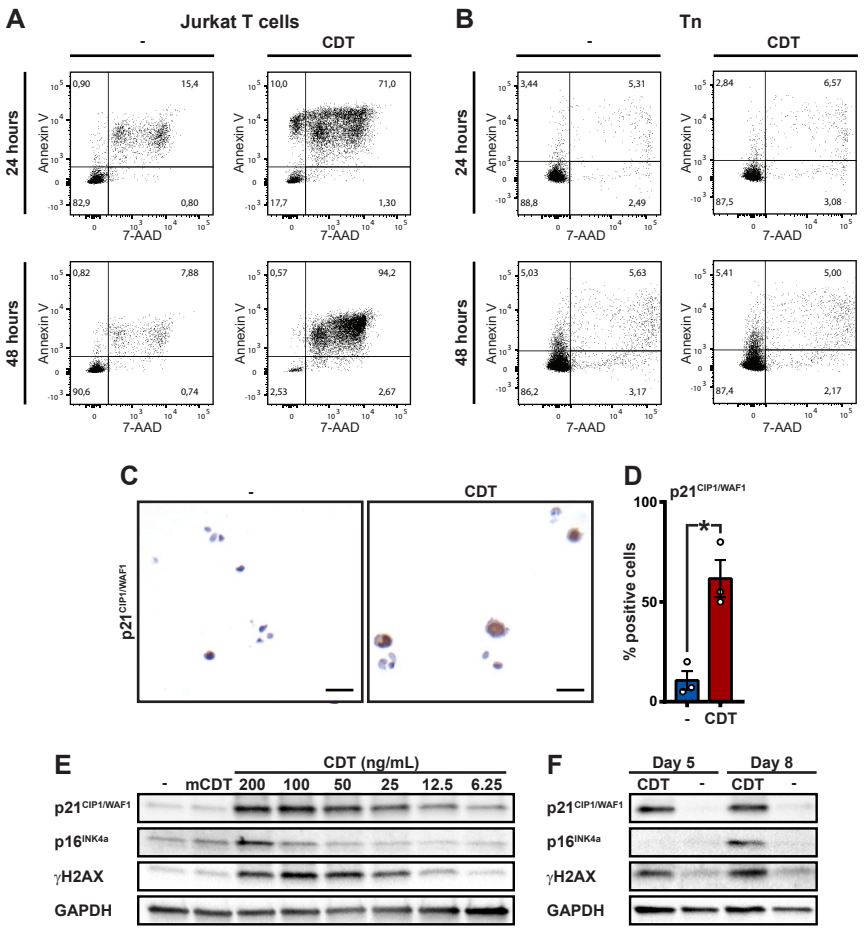


**Figure S2. Jurkat T cells and activated primary CD4 T cells respond differently to CDT intoxication. Related to Figure 2.** (A) Jurkat T cells were cultured in absence (-) or presence of 200 ng/mL CDT for 24 and 48 hours before the percentages of cells positive for the cell death markers Annexin V and 7-AAD were determined by flow cytometry. (B) Naive CD4 T cells (Tn) were cultured with αCD3/CD28 beads in absence (-) or presence of 200 ng/mL CDT for 24 and 48 hours before the percentages of Annexin V- and 7-AAD-positive cells were determined by flow cytometry. (C, D) Tn cells were cultured with αCD3/CD28 beads in absence (-) or presence of 200 ng/mL CDT for 5 days. Subsequently, the cells were analyzed by immunocytochemistry using an antibody against $p21^{CIP1/WAF1}$. (C) Representative picture of the staining showing $p21^{CIP1/WAF1}$ positivity (brown) in the nucleus (blue) of activated Tn cells cultured with CDT. Scale bar corresponds to 50 μm. (D) Histogram summarizing the percentages of $p21^{CIP1/WAF1}$ positive cells from 3 donors. Circles depict the percentages of $p21^{CIP1/WAF1}$-positive cells from individual donors and bars represent the mean ± SEM (*n* = 3). * denotes a significant difference ($p<0.05$) using a paired T-test. (E) Western blot showing the levels of $p21^{CIP1/WAF1}$, $p16^{INK4a}$, γH2AX, and GAPDH in Tn cells cultured for 5 days with αCD3/CD28 beads ± different concentrations of CDT or 200 ng/mL of a catalytically inactive form of CDT (mCDT) harboring a mutation (D273R) in the magnesium-binding site of CdtB. The blot is representative of 2 donors. (F) Western blot showing the levels of $p21^{CIP1/WAF1}$, $p16^{INK4a}$, γH2AX, and GAPDH in Tn cells cultured for 5 and 8 days with αCD3/CD28 beads ± 12.5 ng/mL CDT. The blot is representative of 3 donors.

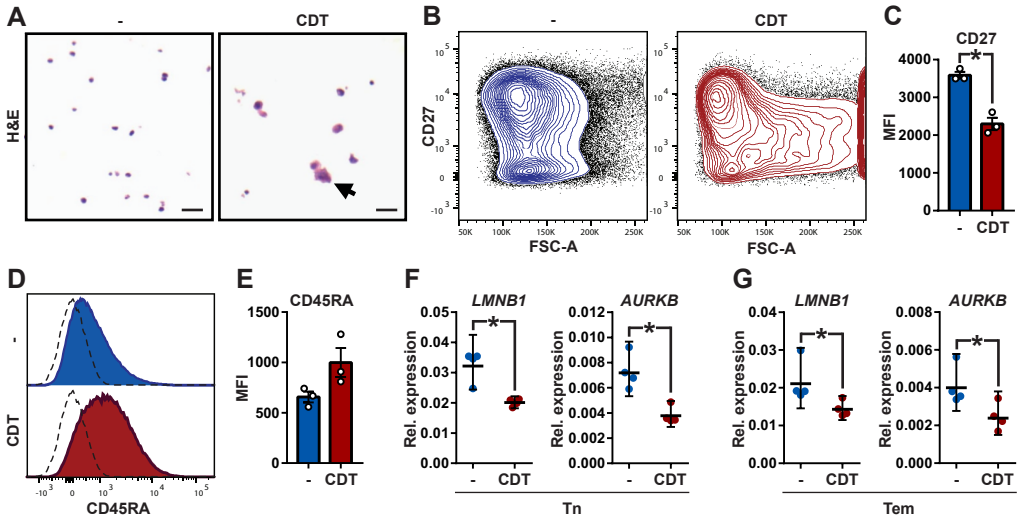


**Figure S3. CDT promotes phenotypic traits of senescence in activated CD4 T cells. Related to Figure 3.** (A) Naive CD4 T cells (Tn) were cultured with αCD3/CD28 beads in absence (-) or presence of 200 ng/mL CDT for 5 days. Subsequently, the cells were stained with hematoxylin and eosin (H&E) to assess cell morphology. The data are representative of 3 donors. Scale bar corresponds to 50 µm. (B-E) Effector memory CD4 T cells (Tem) were cultured with αCD3/CD28 beads in absence (-) or presence of 200 ng/mL CDT for 5 days and analyzed by flow cytometry. (B) Representative contour plots showing the forward-scatter (FSC-A) and CD27 expression. (C) Graph summarizing the expression of CD27 on Tem cells from 3 donors. Circles depict the median fluorescent intensity (MFI) of the individual donors and bars represent the mean MFI ± SEM (*n* = 3). (D) Representative histogram plot showing the expression of CD45RA. Dotted lines represent unstained cells. (E) Graph summarizing the expression of CD45RA on Tem cells from 3 donors. Circles depict the MFI of the individual donors and bars represent the mean MFI ± SEM (*n* = 3). (F, G) Tn and Tem cells were cultured with αCD3/CD28 beads in the absence (-) or presence of 200 ng/mL CDT for 5 days before the relative expression of *LMNB1*, *AURKB*, and *GAPDH* mRNA was analyzed by QPCR. Shown is the expression of *LMNB1* and *AURKB* mRNA relative to that of the reference gene *GAPDH*. Circles represent data points from individual donors, horizontal lines the geometric mean, and error bars the 95% CI (*n* = 4). * denotes a significant difference ($p<0.05$) using a paired T-test.

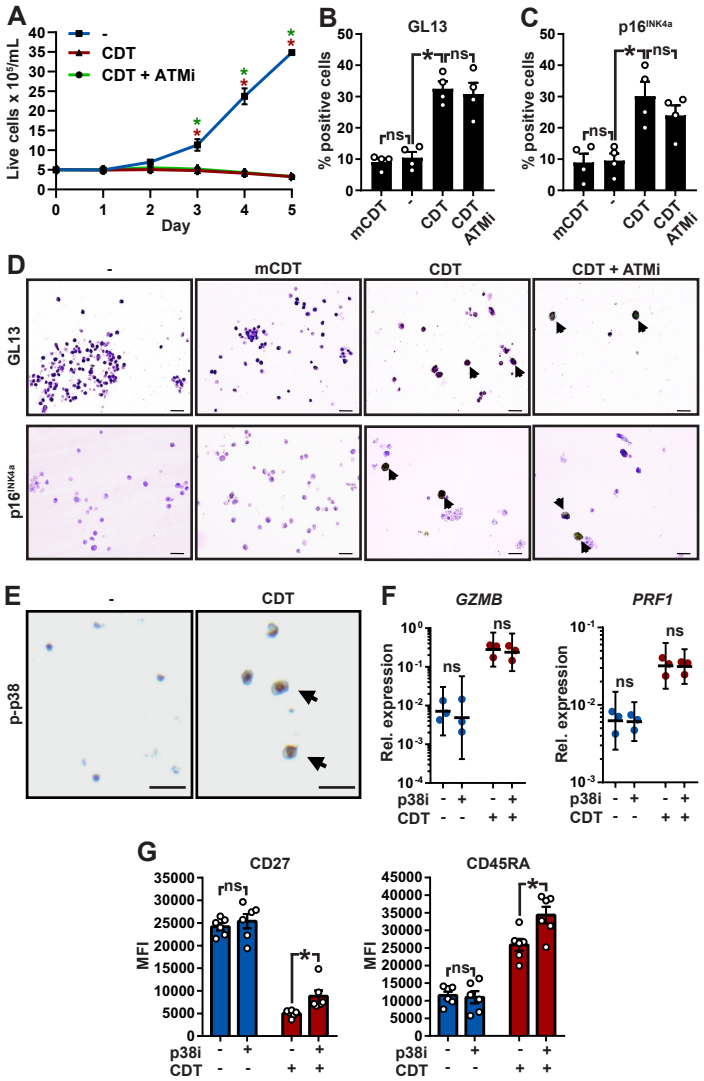


**Figure S4. CDT-induced T cell senescence is not dependent on activation of the ATM-p38 axis. Related to Figure 4.** (A) Tn cells were cultured with αCD3/CD28 beads and either 200 ng/mL CDT, 200 ng/mL CDT + 3μM ATM inhibitor (ATMi, KU-60019), or vehicle (-) for 5 days. The cells were counted every day and the graph depicts the mean concentrations of live cells ± SEM at each time point (*n* = 3). (B-D) Tn cells were cultured with αCD3/CD28 beads and either 200 ng/mL mutated CDT (mCDT), 200 ng/mL CDT, 200 ng/mL CDT + 3μM ATMi, or vehicle (-). After 5 days of culture, the cells were fixed, embedded and analyzed by immunocytochemistry. (B) Histogram showing the percentages of GL13-positive cells. (C) Histogram showing the percentages of $p16^{INK4a}$-positive cells. (B, C) Circles depict data points from individual donors and bars the mean ± SEM (*n* = 4). (D) Representative pictures of Tn cells stained with GL13 and anti-$p16^{INK4a}$ antibody. Arrows denote positive staining (brown color) and scale bars = 20 μm. (E) Representative pictures of activated Tn cells cultured for 5 days ± 200ng/mL CDT followed by immunocytochemical analysis using an antibody against p-p38. Scale bar = 50 μm. (F, G) Tn cells were cultured with αCD3/CD28 beads in the absence (-) or presence of 200 ng/mL CDT. After 48 hours of culture, 10μM p38 inhibitor (p38i, SB203580) or vehicle (-) was added and the cells cultured 72 hours more for a total of 5 days prior analysis. (F) QPCR analysis showing the expression of *GZMB* and *PRF1* mRNA relative to that of the reference gene *GAPDH*. Circles represent data points from individual donors, horizontal lines the geometric mean, and error bars the 95% CI (*n* = 3). (G) Histograms showing the median fluorescent intensity (MFI) of CD27 and CD45RA expression on viable cells as determined by flow cytometry. Circles depict the MFI of individual donors and bars represent the mean MFI ± SEM (*n* = 6). * denotes a significant difference using (A) a 2-way ANOVA with Sidak's multiple comparisons test or (B, C, F, G) a paired T-test and ns denotes no significant difference (p>0.05).

**Table S1. Applied Biosystems pre-designed human TaqMan Gene Expression Assays used in the study. Related to STAR methods**

| Target gene | Target gene name | Cat.# |
|---|---|---|
| *AURKB* | Aurora kinase B | Hs00945858_g1 |
| *CCL1* | C-C motif chemokine ligand 1 | Hs00171072_m1 |
| *CCL3* | C-C motif chemokine ligand 3 | Hs00234142_m1 |
| *CCL4* | C-C motif chemokine ligand 4 | Hs04421399_gH |
| *CCL5* | C-C motif chemokine ligand 5 | Hs00982282_m1 |
| *CDKN1A* | Cyclin dependent kinase inhibitor 1A | Hs00355782_m1 |
| *CDKN2A* | Cyclin dependent kinase inhibitor 2A | Hs00923894_m1 |
| *CSF1* | Colony stimulating factor 1 | Hs00174164_m1 |
| *CSF2* | Colony stimulating factor 2 | Hs00929873_m1 |
| *GAPDH* | Glyceraldehyde-3-phosphate dehydrogenase | Hs02786624_g1 |
| *GZMB* | Granzyme B | Hs00188051_m1 |
| *IFNG* | Interferon gamma | Hs00989291_m1 |
| *IL1B* | Interleukin 1 beta | HS01555410_m1 |
| *IL2* | Interleukin 2 | HS00174114_m1 |
| *IL3* | Interleukin 3 | Hs00174117_m1 |
| *IL4* | Interleukin 4 | HS00174122_m1 |
| *IL5* | Interleukin 5 | HS01548712_g1 |
| *IL6* | Interleukin 6 | HS00985639_m1 |
| *IL7* | Interleukin 7 | Hs00174202_m1 |
| *IL9* | Interleukin 9 | HS00914237_m1 |
| *IL10* | Interleukin 10 | HS00961622_m1 |
| *IL12A* | Interleukin 12A | Hs01073447_m1 |
| *IL13* | Interleukin 13 | Hs00174379_m1 |
| *IL15* | Interleukin 15 | Hs01003716_m1 |
| *IL17A* | Interleukin 17A | Hs00174383_m1 |
| *IL21* | Interleukin 21 | Hs00222327_m1 |
| *IL22* | Interleukin 22 | Hs01574154_m1 |
| *IL23A* | Interleukin 23A | Hs00900828_m1 |
| *IL32* | Interleukin 32 | Hs00992441_m1 |
| *LMNB1* | Lamin B1 | Hs01059210_m1 |
| *MKI67* | Marker of proliferation Ki-67 | Hs04260396_g1 |
| *PFR1* | Perforin 1 | Hs00169473_m1 |
| *TNFA* | Tumor necrosis factor alpha | Hs01113624_g1 |

All TaqMan Gene Expression Assays were purchased from Thermo Fisher Scientific (Waltham, MA, USA)

**Table S2. Primers used for SYBR green QPCR analyses of murine samples. Related to STAR methods.**

| Target gene | Primer name | Sequence (5'-3') |
|---|---|---|
| *GAPDH* | GAPDH-F | AGGTCGGTGTGAACGGATTTG |
| *GAPDH* | GAPDH-R | TGTAGACCATGTAGTTGAGGTCA |
| *IL9* | IL9-F | ATGTTGGTGACATACATCCTTGC |
| *IL9* | IL9-R | TGACGGTGGATCATCCTTCAG |
| *IL13* | IL13-F | CCTGGCTCTTGCTTGCCTT |
| *IL13* | IL13-R | GGTCTTGTGTGATGTTGCTCA |